

E-10-670

STUDY OF VISCOUS FLOW ABOUT AIRFOILS
BY THE INTEGRO-DIFFERENTIAL METHOD

By

James C. Wu, Principal Investigator
and Sarangan Sampath

Georgia Institute of Technology
Atlanta, Georgia 30332

A Final Report for Research Conducted
Under NASA Grant No. NSG 1004

October, 1975

I. INTRODUCTION

This report describes the research performed under NASA Grant No. NSG 1004. The research utilizes an integro-differential method for numerically solving unsteady incompressible viscous flow problems. The method was developed previously by the principal investigator and his co-workers at the Georgia Institute of Technology. During the course of this research, several important advancements were made and incorporated into the solution procedure. Most of these refinements are described in articles that appeared in the open literature (References 1 to 4). A computer program was prepared using the integro-differential method to solve a problem of an impulsively started airfoil. The results for the airfoil problem have not yet appeared in the open literature. This report therefore consists of two parts. In the first part, the work that has been documented in the open literature are summarized. In the second part, some of the results obtained for the airfoil problem are discussed and compared with available information. The second part of this report on the airfoil problem will be supplemented by a Ph.D. thesis being prepared by the second author of this report and by journal articles.

II. THE INTEGRO-DIFFERENTIAL METHOD

The following articles were published as results of research supported by the present grant:

(a) "A Flowfield Segmentation Method for the Numerical Solution of Viscous Flow Problems" by J. C. Wu, A. H. Spring and N. L. Sankar, Proceedings of the Fourth International Conference on Numerical Methods in Fluid Dynamics, pp. 452-457, Springer-Verlag, 1975.

(b) "Integral Representation of Field Variables for the Finite Element Solution of Viscous Flow Problems," Proceedings of the 1974 International Conference on Finite Element Methods in Engineering, pp. 827-840, Clarendon Press, 1974, by J. C. Wu.

(c) "Velocity and Extraneous Boundary Conditions of Viscous Flow Problems," AIAA paper 75-47, 1975, 11 pages, by J. C. Wu.

In the remainder of this part of this report, the integro-differential formulation and the advancements reported in the above listed articles are summarized.

The Integro-Differential Formulation

The Navier-Stokes equations for a fluid with constant density ρ and viscosity ν , and subject to negligible body forces, are expressible in terms of the velocity \vec{v} and the pressure p as

$$\frac{\partial \vec{v}}{\partial t} + (\vec{v} \cdot \nabla) \vec{v} = - \frac{1}{\rho} \nabla p + \nu \nabla^2 \vec{v} \quad (1)$$

Together with the continuity equation

$$\vec{\nabla} \cdot \vec{v} = 0 \quad (2)$$

the equations form a set of four scalar differential equations which are, in principle, sufficient for the determination of \vec{v} and p , provided that adequate initial and boundary conditions are known. Alternative systems of differential equations can be written in terms of the velocity and the vorticity, the stream function and the vorticity, or some other dependent variables. With each of these systems, it has been necessary to compute the values of the dependent variables, usually by means of a finite difference method, for the entire flow field. Associated with this common feature for previous methods there are at least two difficulties in treating problems involving the flow past the exterior of a finite body such as an airfoil, particularly for cases where the shape of the body is not geometrically simple.

The first difficulty arises because the flow region is infinite in extent (at least in the mathematical sense). Consequently, boundary conditions imposed at infinity need to be satisfied. The second, and more serious, difficulty arises because of the large number of discrete data points required in the numerical formulation of complex problems. In particular, for the general problem of flow past a finite body, there are a boundary layer and a separated flow region both embedded in a potential flow. The magnitudes of the velocity gradients differ greatly in these different flow regions. To obtain a sufficiently accurate resolution of the numerical solution in all three flow regions, a large number of discrete grid points must be employed. The data storage

and computer time requirements are, therefore, also large.

It is convenient to introduce, as a dependent variable in the problem, the vorticity vector defined by

$$\vec{\omega} = \vec{\nabla} \times \vec{v} \quad (3)$$

and consider the vorticity transport equation

$$\frac{\partial \vec{\omega}}{\partial t} = \vec{\nabla} \times (\vec{v} \times \vec{\omega}) + \nu \nabla^2 \vec{\omega} \quad (4)$$

which is obtained from equation (1) and describes the convection and diffusion of vorticity with time, t .

The set of equations (2), (3), and (4) partitions the problem conveniently into a kinetic part and a kinematic part.

The kinetic part of the problem deals with the change of the vorticity field $\vec{\omega}$ with time and is described by equation (4). Since equation (4) is parabolic, with known spatial distributions of \vec{v} and $\vec{\omega}$ at any given time τ , the rate of change of $\vec{\omega}$ with time and hence the new distribution of $\vec{\omega}$ at a subsequent time, say $\tau + \Delta\tau$, can be computed. It can be easily seen from equation (4) that, in the computation of the new vorticity values, it is necessary to know the values of velocity at the given time τ only in the region of non-zero vorticity. Since this region of non-zero vorticity is the only region where the flow is rotational and hence the viscous forces are non-zero, the kinetic part of the computation can be confined to the viscous region only.

The kinematic part of the problem relates the velocity distribution $\vec{v}(\vec{r}, t)$ at any given instant to the vorticity distribution $\vec{\omega}(\vec{r}, t)$ at that instant and the velocity conditions at the boundary of the flow

region. This kinematic relation consists of equations (2) and (3) together with prescribed velocity boundary condition. It is expressible as a vector Poisson's equation for the velocity vector

$$\nabla^2 \vec{v}(\vec{r}, t) = - \nabla \times \vec{\omega}(\vec{r}, t) \quad (5)$$

together with the prescribed boundary conditions for \vec{v} . Equation (5) is obtained by taking the curl of equation (3) and using equation (2) to simplify the resulting equation. The vector \vec{r} is the position vector. Since equation (5) is elliptic, the computation of \vec{v} at the neighboring data points. It is, therefore, not possible to compute \vec{v} explicitly (point by point) in the flow field. That is, if equation (5) is used to compute the values of \vec{v} from known values of $\vec{\omega}$ and known boundary conditions, the computation must be performed for the entire flow field, inclusive of the viscous region where $\vec{\omega}$ is non-zero and the inviscid region where $\vec{\omega}$ is zero. Using an integral representation of the velocity vector, however, it becomes possible to evaluate \vec{v} explicitly, point by point. The need to compute \vec{v} in the zero $\vec{\omega}$ region is eliminated.

In the earlier development of the integro-differential method (Reference 6), it has been shown that, for the external flow problem, the integral representation of \vec{v} is

$$\vec{v}(\vec{r}, t) = - \frac{1}{A} \int_R \frac{\vec{\omega}(\vec{r}_o, t) \times (\vec{r}_o - \vec{r})}{|\vec{r}_o - \vec{r}|^d} dR_o + \vec{v}_\infty \quad (6)$$

where in three-dimensional problems $A = 4\pi$ and $d = 3$, in two-dimensional problems $A = 2\pi$ and $d = 2$, in one-dimensional problems $A = 1$ and $d = 1$; \vec{v}_∞ is the free stream velocity; R is the entire region occupied by the

Page 6 Missing from Report

fluid. The no-slip condition, $\vec{v} = 0$ on the solid surface, and the velocity boundary condition infinitely far away from the surface are incorporated into the integral representation (6).

With this integral representation, $\vec{v}(\vec{r}, t)$ can be computed explicitly, i.e., the evaluation of \vec{v} at each data point is accomplished independently of the evaluation of \vec{v} at any other point in the flow field, by numerical quadrature of the integral in equation (6). As a consequence, in the kinematic part of the problem, the computation of \vec{v} can be confined to the viscous region only.

Since, with the integral representation, both the dynamic and the kinematic parts of the problem can be confined to the viscous region of the flow, the number of data points required by the integro-differential method is drastically smaller than that required by current methods treating the kinematic equation in the form of Poisson's equation. For external flow problems, the viscous region usually occupies only a small portion of the entire flow field and the improvement in computational efficiency is particularly dramatic. For example, numerical solutions for a highly complex three-dimensional problem of a jet issuing from a plate and interacting with a crosswind over the plate were successfully obtained using the integro-differential method (Reference 6).

For the external flow problem associated with an immersed solid body whose velocity rises suddenly at an initial time from zero to a constant value, the initial velocity field is given by the potential flow solution everywhere except on the solid surface. The no-slip condition at the solid surface gives rise to an initially concentrated

sheet of vorticity distributed on the surface, the vorticity everywhere else being zero. As time progresses, the vorticity diffuses outward from the surface into the fluid and subsequently also convects with the fluid motion. The integro-differential method allows the time development of both the vorticity and velocity distributions to be followed computationally, offering, in addition to the time-dependent solution, steady state or periodic (Kármán vortex shedding) solutions in the limit of large time (Reference 5).

The ability of the integro-differential method to confine the study of a given problem to the viscous region is distinct from the basic notions of the boundary layer theory, or of the more general matched asymptotic expansion method. With the integro-differential method, the viscous and the inviscid regions are not studied separately. Neither a "matching" nor a "limiting" process is used. The ability to confine the study to the viscous region results not from a simplification of the Navier-Stokes equations but from the use of the integral representation. Since no simplification or approximations other than those involved in the derivation of the Navier-Stokes equations in their differential form are introduced in the integro-differential formulation, the method is valid whether or not appreciable flow separation occurs. Furthermore, no information is lost by confining the computation to the viscous region. The problem of satisfying the boundary condition imposed at infinity is removed. Information about the inviscid region is implicitly contained in the knowledge of the vorticity distribution, which is non-zero only in the viscous region. That is, the velocity in the inviscid region can be computed if desired,

for equation (6) is valid everywhere in the flow field, although in following the development of the flow field with time such computations are unnecessary.

The Flowfield Segmentation Method

The earlier approach of the integro-differential method outlined in the preceding section permits the computational field to be confined to the viscous region. The resulting reduction in the needed number of data points makes the integro-differential method much more efficient than other methods. More recently, it has been shown that a generalized integral representation of the velocity vector further permits the viscous region to be divided into segments of arbitrary shape and size, and the computation to be performed within each segment individually. Error analyses and numerical illustrations show that this flow field segmentation technique leads to further substantial improvement in solution speed and accuracy.

The generalized integral representation is derived from equations (2) and (3) by using a vector potential, Green's theorem for vectors, and principal solution of the Laplace's equation and is

$$\vec{v}(\vec{r}) = -\frac{1}{A} \left[\int_R \frac{\vec{\omega}_o \times (\vec{r}_o - \vec{r})}{|\vec{r}_o - \vec{r}|^d} dR_o + \oint_B \frac{(\vec{v}_o \cdot \vec{n})(\vec{r}_o - \vec{r})}{|\vec{r}_o - \vec{r}|^d} dB_o - \oint_B \frac{(\vec{v}_o \times \vec{n}_o) \times (\vec{r}_o - \vec{r})}{|\vec{r}_o - \vec{r}|^d} dB_o \right] \quad (7)$$

where the subscript "o" denotes that the variable is in the \vec{r}_o space.

This representation is applicable to the internal flow problem as well as to the external flow problem. For the external flow problem, if one considers R to be the entire region occupied by the fluid, then the integrals over B give $-\vec{v}_\infty$ and equation (7) reduces to equation (6). Alternatively, one may consider R to be any portion of the fluid domain. Then, knowing the vorticity distribution in that portion of the fluid domain and the velocity on its boundary, the velocity distribution within that portion can be computed by using equation (7).

This new representation therefore permits the flow field segmentation for the external flow problem as follows:

In the kinetic part of the computation, knowing the distributions of \vec{v} and $\vec{\omega}$ at points interior of and on the boundary of a segment at a given time, new vorticity values within the segment at a subsequent time are computed by numerical solution of the vorticity transport equation (4). Computation of new vorticity values at the boundary points are obtained by either a numerical interpolation, or an explicit finite difference method, or by treating these points as interior points of a different set of segments. Exceptions to the above are the boundary points on solid surfaces or openings where specified velocity boundary conditions enter the problem and only the interpolation method can be used. The degree of accuracy of the boundary-points computation is made compatible with that of the interior point computation.

In the kinematic part of the computation, new values of the velocity at the boundary points are computed from the new vorticity distribution explicitly by numerical quadrature of the integral

representation (6). With the new velocity at boundary points and new vorticity at the interior and boundary points determined, the computation of the new velocity values for the interior points can be performed either by the numerical quadrature of the integral representation (7) or by a numerical solution of the Poisson's equation.

The advantage of employing the segmentation method can be easily seen from the different numbers of algebraic operations needed for computing each velocity value using the integral representation. For illustration, consider the two-dimensional flow problem. By mapping the solution field into finite-elements, one obtains the following formula for numerical quadrature from equation (6):

$$v_{\ell,i} = \sum_{j=1}^N F_{\ell,ij} \omega_j + v_{\ell,\infty} \quad (8)$$

where " ℓ " denotes the ℓ th component of \vec{v} and is either 1 or 2, " i " refers to the node for which the value of v_{ℓ} is to be computed; " j " refers to any non-zero vorticity node; $F_{\ell,ij}$ are geometric functions depending on the relative positions of the nodes i and j ; N is the total number of non-zero vorticity nodes in the flowfield R . Similarly, one obtains from equation (7):

$$v_{\ell,i} = \sum_{j=1}^Q F_{\ell,ij} \omega_j + \sum_{m=1}^2 \sum_{k=1}^P G_{m,ik} v_{m,k} \quad (9)$$

where $G_{m,ik}$ are geometric functions depending on the relative positions of the node i and the node k which is located on the compartment boundary;

Q is the number of non-zero vorticity in the region R ; and P is the number of boundary nodes on B . If there are 4000 nodes on which the values of vorticity and its derivatives are non-negligible, then velocity components need to be computed only for these 4000 nodes. Without the segmentation of the solution field, one would use equation (8) to compute the velocity values. Since $N = 4000$, the computation of each velocity value requires the multiplication of 4000 values of the geometric function $F_{\ell,ij}$ with 4000 values of the vorticity ω_j and the addition of the products. For the 4000 nodes (and therefore 8000 velocity values), a total of 3.2×10^6 multiplications and 3.2×10^6 additions are needed for the velocity computation. With the solution field segmented, one first uses equation (8) to compute the velocity values at nodes on the boundary of the compartments. This portion of the velocity computation still requires 4000 multiplications and 4000 additions for each velocity value. However, for the computation of velocity values at nodes interior nodes, equation (9) is now used and the required number of multiplications and additions reduces to $Q + 2P$ for each velocity value. For example, with a compartment containing a total of 400 nodes, 80 of which are on the boundary of the compartments, only 560 multiplications and additions are now required for computing each velocity value at an interior node. Obviously, the segmentation of the solution field offers a very drastic improvement in solution speed. This improvement can, in fact, be made even greater by the use of successive segmentation. That is, one may first compute the velocity values on boundaries of larger compartments each containing, say, 2000 nodes. Once this is accomplished, the computation of the velocity

values on the boundaries of the 400-node compartments (but are interior of the 2000-node compartments) can be accomplished much more rapidly.

The flow field segmentation technique utilizes the most important feature of the integro-differential method, i.e., the ability to confine the computational field to the viscous flow region only, and adds a great flexibility to the method. Since the segments can be of arbitrary shape and size, simple shapes (e.g., rectangular, triangular, circular shapes) can be utilized. Consequently, methods which possess great speed and accuracy but are difficult to apply in problems of complex solid body shapes can be readily incorporated in the computational procedures. For example, the fast Poisson solvers can be used in the proposed work in the kinematic computation of the velocity at the interior point of each segment. The alternating direction implicit method can be used for the dynamic computation of the vorticity. Furthermore, since the computation is performed individually within each segment, the use of variable grid spacing is straightforward. Thus, for the segments adjacent to the solid body where the velocity and vorticity gradients are expected to be large, closely spaced grid points can be used to obtain sufficient solution resolution.

Numerical results obtained utilizing the segmentation method are found to be practically identical to those obtained without using segmentation. The results, discussed in more detail in Ref. 1, also show that very drastic reduction in needed computer time resulted from the use of the segmentation technique, as was expected.

Farfield Boundary Condition

It is shown in Reference 3 that, for the external flow problem, the difficulty of satisfying the freestream velocity boundary condition at an infinite distance from the solid body is completely removed by the use of the integro-differential formulation. If the solid body is not rotating, but is merely translating at a velocity $-\vec{v}_{\infty}$ (which may be time-dependent) relative to the freestream, then equation (6) is applicable. The contribution of the freestream velocity boundary condition to the velocity field is simply \vec{v}_{∞} . The vorticity $\vec{\omega}$ in the fluid originates from the solid surface and, at any finite time τ , is non-negligible only within a finite distance from the solid surface. Thus the contribution of the integral in equation (6) to the velocity field is zero at infinity. That is, with equation (6), the freestream velocity boundary condition is satisfied exactly at an infinite distance from the solid body.

In Reference 3, the importance of the "farfield" velocity boundary condition is illustrated by numerical examples. In addition, integral expressions for the velocity vector are derived for the more general case where the solid body is undergoing both translation and rotation. It is shown in Reference 3 that the "farfield" velocity boundary condition is satisfied exactly by the integral expressions for this more general case.

Extraneous Boundary Condition

The kinetic processes of vorticity diffusion and convection in an incompressible fluid is described by equation (4), the vorticity

transport equation. This equation is parabolic in its time-space relation and is valid in the fluid domain R . In order to solve equation (4) and obtain the time dependent vorticity field $\vec{\omega}(\vec{r}, t)$ in the fluid domain R , the values of $\vec{\omega}$ on the boundary B must be known as a function of time. The boundary B may contain a solid boundary S . The "boundary values" of $\vec{\omega}$ on S may not be computed by solving equation (4) since the local "generation" or "depletion" of vorticity on S is not described by the kinetic processes of vorticity transport. Since the specification of vorticity values on S apparently overspecifies the problem, the expression "extraneous boundary condition" is used to describe this difficulty.

In most of the previous investigations, various one-sided difference formulae have been used to estimate the vorticity values on solid boundaries from the no-slip condition and the computed velocity (or stream function) values at grid points near the boundary. It has been found that difference formulae of first-order accuracy tend to yield stable solutions while second-order formulae tend to give unstable results at high Reynolds numbers. In fact, for some problems, second order formulae, even when stable, gave less accurate solutions than did the first-order formulae. The use of first-order formulae, however, restricts the over-all accuracy of the solution. There existed, therefore, considerable uncertainties regarding the correct one-sided formulae to use and the limitations of each formula.

With the integral representation for the velocity vector, it becomes possible to compute the vorticity values on S accurately based on kinematic considerations alone. In Reference 3, it is demonstrated

that this new approach correctly simulates the physical process of vorticity "generation" on the solid surface S and therefore removes the difficulty of extraneous boundary condition.

The kinematic aspect of the viscous flow problem relates the velocity distribution at any given instant of time to the vorticity distribution at that instant, and vice versa. If the velocity field is known, then the vorticity field is uniquely determined on the basis of equation (3). On the other hand, if the vorticity field is known throughout an unbounded region, then the velocity field is uniquely determined on the basis of equation (6). It is obvious that the stress-strain relation, which differentiates the kinetic behavior of a solid from that of a fluid, does not enter into the kinematic relationship between the instantaneous vorticity and velocity fields. Therefore, equation (6) is valid in both the fluid domain and the domain occupied by the solid. In other words, as far as the kinematics of the problem is concerned, one may replace the solid by a fluid moving at the instantaneous velocity of the solid. In a reference frame attached to the solid, the velocity inside the region occupied by the solid happens to be zero. The vorticity in the solid region is therefore also zero. As a consequence, the velocity field is uniquely determined by equation (6) both in the fluid domain R and in the solid domain R' provided that the vorticity field is known throughout the fluid domain R . The kinematic relation requires that this vorticity field must be such that the velocity field as determined by equation (6) is zero everywhere inside the solid domain R' . Clearly, not all vorticity fields in R would give zero velocity values throughout R' . In other words, the

vorticity field in R is subject to a kinematic restriction.

One notes that, in addition to this kinematic restriction, the vorticity field in the fluid domain R , except at the fluid-solid interface S^+ , is determined by the kinetic process of vorticity transport. As a consequence, the fact that the velocity field is zero in the solid domain R' places a kinematic restriction only on the vorticity distribution at the surface S^+ . This restriction, in fact, gives rise to the phenomena commonly referred to as the generation or depletion of vorticity on the solid surface.

In Reference 3, it is found that for two-dimensional flows, if a vorticity field in R is found such that either the normal component or the tangential component of the velocity is zero on the solid surface S , then both velocity components are zero in the entire region R' bounded externally by S . As a consequence, to establish the extraneous vorticity boundary condition on S^+ , one needs only to search for a vorticity distribution on S^+ which, when combined with the known (from the kinetics) vorticity field everywhere in R except S^+ , gives either zero normal velocity on S or zero tangential velocity on S . In other words, for the external flow problem, equation (6) is rewritten as

$$\vec{v}(\vec{r}, t) = -\frac{1}{2\pi} \int_{R-S^+} \frac{\vec{\omega}_0 \times (\vec{r}_0 - \vec{r})}{|\vec{r}_0 - \vec{r}|^2} dR_0 - \frac{1}{2\pi} \int_{S^+} \frac{\vec{\zeta}_0 \times (\vec{r}_0 - \vec{r})}{|\vec{r}_0 - \vec{r}|^2} dS_0 + \vec{v}_\infty \quad (10)$$

where $\vec{\zeta}_0$ is a surface distribution of vorticity on S^+ , treated separately from the remaining vorticity field in the region $R - S^+$. The vector equation (10) gives two scalar component equations. With the velocity

boundary condition specified on S and the vorticity distribution in the region $R - S^+$ known, the application of equation (10) at each boundary point gives two equations, one for the normal velocity and one for the tangential velocity, both containing the values of ζ on the boundary points as unknowns. If N boundary points are used in the numerical procedure, then the application of equation (10) at the N points gives a set of $2N$ algebraic equations containing N unknown values of ζ . However, since one needs only to satisfy either the normal velocity boundary condition or the tangential velocity boundary condition, only N algebraic equations are needed in the computation.

It is further shown that for an internal flow problem, the solution of the N algebraic equations exists and is unique. For an external flow problem, however, the solution of the N algebraic equations is not unique. The coefficient matrix of the N equations is in fact of rank $N - 1$. It is shown that for this external flow problem a unique distribution of the vorticity on the solid boundary is obtainable from the integral representation for the velocity vector and the integral law for vorticity. The analyses for the three-dimensional and interior flow problems are similar to those given here for the two-dimensional exterior problem. In fact, they are slightly less involved since for the two-dimensional exterior problems the flowfield is doubly connected and for the other problems the flowfield of concern is simply connected. It is worthwhile noting that the well accepted method for initiating the time-dependent viscous flow computations is to assume that the solid is set into motion impulsively, obtain a potential flow solution, and compute the initial vorticity distribution (which is non-zero only

at the solid boundary) from the tangential velocity of the potential flow on the boundary. The initial vorticity distribution is thus determined from the kinematical aspect of the problem. This method for initiating the computation is in fact a specialization of the present method to the case where the vorticity is non-zero only at the boundary.

The present method does away with the need of using one-sided difference formula. It allows the generation (or depletion) of vorticity at the solid boundary to be followed computationally using kinematic relations only. The present method ensures the satisfaction of the principle of total vorticity conservation and of the specified velocity boundary conditions at all data points on the solid boundary. With a one-sided difference formula, the no-slip condition is applied individually at each grid point on the solid boundary and a vorticity value is obtained for that point. Each vorticity value thus computed, however, gives rise to a finite velocity at all the other boundary nodes. The sum of the contributions of boundary vorticities does not in general vanish at any of the boundary nodes. Thus, in reality, there is no assurance that either the velocity boundary condition is satisfied or the total vorticity is conserved.

It should be noted that Lighthill (Reference 8) described an approach which appears to be similar to that described here. In reality, however, there are substantial differences between Lighthill's approach and the present work. These differences shall be explained in a future article. Thus far, with Lighthill's approach, it was only possible to treat problems involving simple two-dimensional geometries such as circles and flat plates. The present approach has been used in

the study of problems involving more complex geometries, including the three-dimensional problem of a jet issuing normally from a plate into a crossflow (Reference 6). Numerical illustrations are provided in Reference 3.

Integral Representation for Compressible Flows

In Reference 2, an integral representation is presented for the kinematics of compressible flow. This integral representation is

$$\vec{v}(\vec{r}, t) = -\frac{1}{A} \left[\int_R \frac{b_o(\vec{r}_o - \vec{r}) + \vec{\omega}_o \times (\vec{r}_o - \vec{r})}{|\vec{r}_o - \vec{r}|^d} dR_o - \int_{S'} \frac{(\vec{v}_s \cdot \vec{n}_o)(\vec{r}_o - \vec{r}) - (\vec{v}_s \times \vec{n}_o) \times (\vec{r}_o - \vec{r})}{|\vec{r}_o - \vec{r}|^d} dS_o \right] \quad (11)$$

where

$$b = \vec{\nabla} \cdot \vec{v}$$

is the dilatation of the fluid.

Reference 2 describes a procedure for computing time-dependent viscous compressible flows using the integral representation (11).

Integral Representation for the Kinetics of Steady Incompressible Flow

In addition to the integral representation for the kinematics of compressible flow, it was found that for steady flows, the kinetic aspect of incompressible flow can also be recast into the form of an integral representation -- for the vorticity vector. The result is, for the steady incompressible flow problem, a system of integral equations

ideally suited for the finite-element approach. Each integral equation is an integral representation of a field variable. In the derivation of the integral equations, neither the existence of a variational principle nor a weighted residual (or Galerkin's) approach is required. The application of the finite element method is therefore independent of a minimization of functionals. This new formulation for the steady flow problem retains the distinguishing feature of the integro-differential formulation for time-dependent flows -- the computation field can still be confined to the viscous region only. A method for computing steady flows based on the new formulation is described in Reference 2. Some numerical results are presented.

III. FLOW PAST AN IMPULSIVELY STARTED AIRFOIL

This part of this report describes the work that has been carried out in obtaining a numerical solution of the incompressible viscous flow past an impulsively started 9% thick symmetric Joukowski airfoil at an angle of attack of 15° and a Reynolds number of 1000. This problem was studied previously by Mehta (Reference 7) who mapped the fluid domain into the interior of a unit circle and used the vorticity and stream function as the primary variables.

To facilitate a comparison between the results of this research and the results of Mehta, the integral representation and the vorticity transport equation presented earlier in terms of the velocity and the vorticity are modified and reformulated in terms of the vorticity and the stream function in Mehta's transformed plane. Results are obtained by numerically solving the resulting integro-differential equations for some early time levels and compared with that of Reference 7.

Coordinate Transformations

The shape of the 9% symmetric Joukowski airfoil is given in Figure 1 in the complex plane $z = x + iy$. By using the conformal transformation

$$z = \frac{1}{\kappa} + \gamma + \frac{\kappa C^2}{1 + \gamma\kappa} \quad (12)$$

where $\kappa = re^{i\theta}$, C and γ are real constants, the airfoil surface transforms into a circle and the exterior of the airfoil, i.e., the fluid

domain, is mapped in the κ plane as the interior of the circle.

The coordinates of the z -plane and κ -plane are related by

$$x = \left(1 + \frac{C^2 r^2}{f^2} \right) \left(\frac{\cos \theta}{r} + \gamma \right) \quad (13)$$

$$y = \frac{\sin \theta}{r} \left(\frac{C^2 r^2}{f^2} - 1 \right) \quad (14)$$

where

$$f^2 = 1 + \gamma^2 r^2 + 2\gamma r \cos \theta \quad (15)$$

The scale factor H is given by

$$H = \left| \frac{dz}{d\kappa} \right| = \left[\left(\frac{1}{r^2} - \frac{C^2}{f^2} \right)^2 + \frac{4 C^2}{r^2 f^4} \sin^2 \theta \right]^{\frac{1}{2}} \quad (16)$$

where

$$f^2 = 1 + \gamma^2 r^2 + 2\gamma r \cos \theta \quad (17)$$

For the present problem, the values of C and γ are taken to be 0.9241635 and - 0.05214 respectively. The coordinates and the flow variables are to be non-dimensionalized with respect to the radius of the circle and the freestream velocity. Therefore the airfoil in the z plane transforms into a unit circle in the κ plane. The non-dimensional chord length, L , of the airfoil is, according to equation (12), 3.71281277 . The airfoil is 9.9998% thick.

A non-conformal transformation is utilized to obtain an efficient distribution of grid points for computation. The θ coordinate in the κ plane is not modified. The r coordinate was "stretched" by the relation

$$\rho = \frac{1}{4.8} [\tanh^{-1} (1.996590918 r - 1.032563339) + 2.8] \quad (18)$$

This transformation maps the annular region between $r = 0.02$ and $r = 1$ in the κ -plane into the interior of a unit circle in the ρ - θ plane.

In Reference 7, both the kinematic and kinetic equations are expressed in their differential form in the ρ - θ plane. Finite difference methods are then used to obtain numerical solutions. In the present work, the kinetic equation, i.e., the vorticity transport equation, is expressed in the differential form in the ρ - θ plane. The kinematic equation, i.e., the Poisson's equation, is recast into an integral representation for the stream function in the κ plane, as discussed in the following section.

Governing Equations

The vorticity equation expressed in terms of non-dimensional variables in the ρ - θ plane is

$$\begin{aligned} r^2 H^2 \frac{\partial \omega}{\partial t} = r \rho' \left(\frac{\partial \psi}{\partial \theta} \frac{\partial \omega}{\partial \theta} - \frac{\partial \psi}{\partial \theta} \frac{\partial \omega}{\partial \rho} \right) \\ + \frac{L}{R} \left[(r \rho')^2 \frac{\partial^2 \omega}{\partial \rho^2} + r(\rho' + r \rho'') \frac{\partial \omega}{\partial \rho} + \frac{\partial^2 \omega}{\partial \theta^2} \right] \end{aligned} \quad (19)$$

where

$$\rho' = \frac{d\rho}{dr} \quad \text{and} \quad \rho'' = \frac{d^2 \rho}{dr^2}$$

The Poisson's equation in the κ plane is

$$\frac{\partial^2 \psi}{\partial r^2} + \frac{1}{r} \frac{\partial \psi}{\partial r} + \frac{1}{r^2} \frac{\partial^2 \psi}{\partial \theta^2} = -\omega f^2 \quad (20)$$

In Reference 7, equation (20) is re-expressed in the ρ - θ plane. "Farfield" boundary conditions for the stream function is then used at the boundary $\rho = 0$, which corresponds to $r = 0.02$ in the κ -plane and roughly corresponds to a circle of radius $13L$ in the z plane (the physical plane). In the present study an integral representation for ψ is derived and the freestream condition is satisfied infinitely far from the airfoil (i.e., at $r = 0$).

In general, the Poisson's equation can be recast into an integral representation for the dependent variable by the use of the Green's theorem and a principal solution of the Laplace's equation (Reference 5). For two-dimensional problems, the principal solution corresponds to a logarithmic potential (Reference 9). The integral representation for the Poisson's equation in the z plane, $\nabla^2 \psi = -\omega$, is

$$\psi(z) = \int_R \int \omega_o f dR_o + \oint_B \left[\left(\frac{\partial \psi}{\partial n} \right)_o f - \psi_o \frac{\partial f}{\partial n_o} \right] dB_o \quad (21)$$

where

$$f = \frac{1}{2\pi} \ln \frac{1}{|z - z_o|} \quad (22)$$

is the principal solution in the z plane.

Using the prescribed boundary conditions,

$$\frac{\partial \psi}{\partial n} = 0 \quad \text{on the solid surface } S \quad (23)$$

$$\frac{\partial \psi}{\partial y} = U_{\infty} \quad \text{infinitely away from } S \quad (24)$$

$$\frac{\partial \psi}{\partial x} = -V_{\infty}$$

it can be shown that the second integral in equation (21) reduces to $U_{\infty} y - V_{\infty} x$. Therefore one has

$$\psi(z) = \int \int_R \omega_0 f \, dR_0 + U_{\infty} y - V_{\infty} x + C_1 \quad (25)$$

where C_1 is an arbitrary constant.

With any conformal transformation $z = g(\kappa)$, the transformed Poisson's equation is

$$\nabla_{\kappa}^2 \psi = -\omega H^2 \quad (26)$$

where H is the scale factor and the subscript κ denotes differentiations in the κ plane.

Equation (26) is still a Poisson's equation. It differs from the Poisson's equation in the z plane only by the fact that the inhomogeneous term in the transformed equation is $-\omega H^2$ in place of $-\omega$. Thus, one may let

$$\omega_{\kappa} = \omega H^2 \quad (27)$$

and write

$$\psi(\kappa) = \iint_{R_\kappa} w_{\kappa_0} f_\kappa dR_0$$

$$+ \oint_{B_\kappa} \left[\left(\frac{\partial \psi}{\partial n_\kappa} \right)_0 f_\kappa - \psi_0 \frac{\partial f}{\partial n_{\kappa_0}} \right] dB_0 \quad (28)$$

where

$$f_\kappa = \frac{1}{2\pi} \ln \frac{1}{|\kappa_0 - \kappa|}$$

and the subscript " κ " refers to the κ plane, e.g., R_κ is the region in the κ plane that corresponds to the region R in the z -plane. If the transformation is such that the scale factor approaches unity for large values of z , then the streamlines at great distance from S are not distorted by the transformation. The surface integrals in equation (28) then give $U_\infty \eta - V_\infty \xi$, where ξ and η are respectively the abscissa and ordinate in the transformed plane. In the present study, the exterior of the airfoil is transformed into the interior of a unit circle in the κ -plane. The contribution of the surface integral in equation (28) must therefore be analyzed separately.

Consider the surface S' to be a circle of radius A centered about the origin, with $A \rightarrow \infty$. The surface S' encloses the airfoil in the z plane. The stream function on S' is $U_\infty y - V_\infty x$. In the transformed plane κ , S'_κ is a circle of radius ϵ centered about the origin, with $\epsilon = 1/R \rightarrow 0$. Since ψ is a scalar and is invariant to the transformation, one obtains from equation (24),

$$\frac{\partial \psi}{\partial n} = -\frac{1}{r^2} (U_\infty \sin \theta + V_\infty \cos \theta) \quad (29)$$

Together with the boundary conditions on S , the surface integral in equation (28) gives $-1/4(U_\infty \sin \theta + V_\infty \cos \theta)$. Equation (28) thus becomes

$$\begin{aligned} \psi(\kappa) = & \frac{1}{2\pi} \int \int_{R_\kappa} \omega_{\kappa_0} \ln \frac{1}{|\kappa - \kappa_0|} dR_0 \\ & - \frac{1}{r} (U_\infty \sin \theta + V_\infty \cos \theta) + C_{1\kappa} \end{aligned} \quad (30)$$

The arbitrary constant $C_{1\kappa}$ is the value of the stream function outside the unit circle in the κ plane. It is also the value of the stream function inside the airfoil in the z plane. The value of $C_{1\kappa}$ can be set to be zero and equation (30) can be more conveniently re-written as

$$\begin{aligned} \psi(\kappa) = & \frac{1}{2\pi} \int \int_{R_\kappa} \omega_{\kappa_1} \ln \frac{|\kappa|}{|\kappa - \kappa_0|} dR_0 \\ & - \frac{1}{r} (U_\infty \sin \theta + V_\infty \cos \theta) \end{aligned} \quad (31)$$

for reasons to be explained shortly.

Although it is possible to re-express equation (31) in the ρ - θ plane, for computational purposes it is more convenient to use equation (31). In the present study, therefore, equation (31) is used.

Extraneous Boundary Condition

The vorticity distribution ω_κ in the κ plane is restricted kinematically by the requirement that $\psi = 0$ exterior of the unit circle. (Note that this region corresponds to the domain of the solid in the z plane.) At any given instant of time, the vorticity distribution away from the fluid-solid interface is determined by the kinetics of the problem. The kinematic restriction therefore applies only to the vorticity distribution on the fluid-solid interface at that instant of time. In Reference 5, an implicit method utilizing the integral representation (6) is presented. The method is specifically developed for the problem formulated in terms of the vorticity and the velocity. It requires the numerical solution of a system of N simultaneous algebraic equations involving unknown vorticity values at boundary points on the interface. In the following, an explicit method for the computation of the surface vorticity values is described. This new method is useful both for the vorticity-velocity formulation and for the vorticity-stream function formulation.

The differential equations describing the kinematic relation between the vorticity and the stream function (or velocity) are linear. Therefore the method of superposition is useful in computing the extraneous boundary condition. If one separates the vorticity on the surface S_κ from that in the region R_κ but not on S , then equation (31) becomes

$$\psi(\kappa) = \frac{1}{2\pi} \int \int_{R_\kappa - S_\kappa} \omega_{\kappa_0} \ln \frac{|\kappa|}{|\kappa - \kappa_0|} dR_0 + \frac{1}{2\pi} \int_{S_\kappa} \zeta_{\kappa_0} \ln \frac{|\kappa|}{|\kappa - \kappa_0|} dS_{\kappa_0}$$

$$-\frac{1}{r} (U_{\infty} \sin \theta + V_{\infty} \cos \theta) \quad (32)$$

where ζ_{κ} is a surface distribution of vorticity, its dimension being that of vorticity times length. Let us consider ζ_{κ} in two parts

$$\zeta_{\kappa} = \zeta_{\kappa 1} + \zeta_{\kappa 2} \quad (33)$$

where $\zeta_{\kappa 1}$ is the contribution of the freestream condition to the surface vorticity and $\zeta_{\kappa 2}$ is the contribution of the vorticity away from S_{κ} to the surface vorticity.

The surface vorticity distribution corresponding to a potential flow past a circular cylinder is readily available in standard texts. Upon conformally mapping the exterior of the circle into the interior of a unit circle, one finds,

$$\zeta_{\kappa 1} = 2(U_{\infty} \sin \theta + V_{\infty} \cos \theta) \quad (34)$$

The stream function associated with the surface vorticity distribution $\zeta_{\kappa 1}$, as given above, shall now be determined for the region $r \geq 1$. (Note that $\kappa = re^{i\theta}$, and that the region $r \geq 1$ corresponds to the domain occupied by the airfoil.) From equation (32), this stream function is

$$\begin{aligned} I_1 &= \frac{1}{\pi} \int_0^{2\pi} (U_{\infty} \sin \theta_0 + V_{\infty} \cos \theta_0) \ln \frac{1}{[r^2 + 1 - 2r \cos(\theta_0 - \theta)]^{\frac{1}{2}}} d\theta_0 \\ &= -\frac{Q}{2\pi} \int_0^{2\pi} \sin(\theta_0 + \alpha) \ln [r^2 + 1 - 2r \cos(\theta_0 - \theta)]^{\frac{1}{2}} d\theta_0 \quad (35) \end{aligned}$$

where $Q = (U_\infty^2 + V_\infty^2)^{\frac{1}{2}}$ is the freestream velocity magnitude and $\alpha = \tan^{-1} V_\infty/U_\infty$. Integrating by parts, one then obtains

$$I_1 = -\frac{Qr}{\pi} \int_0^{2\pi} \frac{\cos(\theta_0 + \alpha) \sin(\theta_0 - \theta)}{r^2 + 1 - 2r \cos(\theta_0 - \theta)} d\theta_0$$

Letting $\beta = \theta_0 - \theta$, one has

$$I_1 = -\frac{Qr}{\pi} \int_\theta^{2\pi-\theta} \frac{[\cos \beta \cos(\theta + \alpha) - \sin \beta \sin(\theta + \alpha)] \sin \beta}{r^2 + 1 - 2r \cos \beta} d\beta$$

The odd part of the integrand above does not contribute to the integral. The even part of the integrand is periodic in β with the period 2π . One therefore has

$$\begin{aligned} I_1 &= \frac{Qr \sin(\theta + \alpha)}{\pi} \int_0^\pi \frac{2 \sin^2 \beta}{r^2 + 1 - 2r \cos \beta} d\beta \\ &= \frac{Qr \sin(\theta + \alpha)}{\pi} \left[\int_0^\pi \frac{d\beta}{r^2 + 1 - 2r \cos \beta} - \int_0^\pi \frac{\cos 2\beta}{r^2 + 1 - 2r \cos \beta} d\beta \right] \quad (36) \end{aligned}$$

Explicit expressions for the definite integrals in equation (36) are available in standard mathematical tables. For $r > 1$, one has

$$I_1 = \frac{Q}{r} \sin(\theta + \alpha) = \frac{1}{r} (U_\infty \sin \theta + V_\infty \cos \theta) \quad (37)$$

Thus the contribution of $\zeta_{\kappa 1}$ to the stream function value is the negative of the freestream contribution to the stream function (the last part of equation 32). It is easy to show that $\int_0^{2\pi} \zeta_{\kappa 1} d\theta = 0$ so that $\zeta_{\kappa 1}$ does not contribute to the total vorticity.

Let $d\zeta_{\kappa 2}$ be the contribution of the elementary vorticity $\omega_{\kappa 0} dR_{\kappa 0}$ located at κ_0 to the surface vorticity distribution $\zeta_{\kappa 2}$. By the method of images, one finds

$$d\zeta_{\kappa 2} = \frac{(r_o^2 - 1) \omega_{\kappa 0} dR_{\kappa 0}}{2\pi[1 + r_o^2 - 2r_o \cos(\theta_o - \theta)]} \quad (38)$$

By the use of the method of residues, it can be shown that the stream function associated with $d\zeta_{\kappa 2}$ is exactly opposite to that associated with $\omega_{\kappa 0} dR_{\kappa 0}$. Therefore the combined contributions of $d\zeta_{\kappa 2}$ and of $\omega_{\kappa} dR_{\kappa}$ to the stream function is zero inside the airfoil. Furthermore,

$$\int_0^{2\pi} \frac{(r_o^2 - 1) \omega_{\kappa 0} dR_{\kappa 0}}{2\pi[1 + r_o^2 - 2r_o \cos(\theta_o - \theta)]} d\theta_o = - \omega_{\kappa 0} dR_{\kappa 0} \quad (39)$$

$d\zeta_{\kappa 2}$ together with $\omega_{\kappa 0} dR_{\kappa 0}$ do not contribute to the total vorticity.

Obviously, if one lets

$$\zeta_{\kappa 2} = \int d\zeta_{\kappa 2} = \frac{1}{2\pi} \int \int_{R_{\kappa} - S_{\kappa}} \frac{(r_o^2 - 1) \omega_{\kappa 0} dR_{\kappa 0}}{[1 + r_o^2 - 2r_o \cos(\theta_o - \theta)]}$$

then the combined contributions of $\zeta_{\kappa 2}$ and ω_{κ} distributed in $R_{\kappa} - S_{\kappa}$ to the stream function is zero in the region $r > 1$ (inside the airfoil). Furthermore, $\zeta_{\kappa 2}$ together with the vorticity away from S gives zero total vorticity. One therefore has

$$\zeta_{\kappa} = \frac{1}{2\pi} \int \int_{R_{\kappa} - S_{\kappa}} \frac{(r_o^2 - 1) \omega_{\kappa 0} dR_{\kappa 0}}{[1 + r_o^2 - 2r_o \cos(\theta_o - \theta)]} + 2(U_{\infty} \sin \theta + V_{\infty} \cos \theta) \quad (40)$$

Clearly, the surface vorticity distribution given by equation (40) satisfied both the kinematic requirement that the stream function inside the airfoil is zero and the principle of total vorticity conservation. It permits the explicit, point by point, computation of the surface vorticity values.

Farfield Velocity Boundary Condition

It can be shown that for $r < 1$, equation (36) gives

$$I_1 = r(U_\infty \sin \theta + V_\infty \cos \theta)$$

so that I_1 is zero at the origin. Furthermore, the combined contributions to the stream function of $\zeta_{\kappa 2}$ and the vorticity distributed in $R_\kappa - S_\kappa$ is zero at the origin. Since the origin in the κ plane corresponds to a surface infinitely far from S in the physical plane z , the freestream condition $\psi = -1/r(U_\infty \sin \theta + V_\infty \cos \theta)$ (or $\psi = U_\infty y - V_\infty x$ in the z plane) is satisfied exactly at infinity in the z plane.

Aerodynamic Loads

On the surface S the velocity vector vanishes and the Navier-Stokes equations reduce to

$$\vec{\nabla}_p = \frac{\rho L}{R} \nabla^2 \vec{v} = -\frac{\rho L}{R} \vec{\nabla} \times \vec{\omega} \quad (41)$$

The tangential component of this equation is, in the κ plane,

$$\frac{\partial p}{\partial \theta} = \frac{L}{R} \frac{\partial \omega}{\partial r} = \frac{L}{R} \rho' \frac{\partial \omega}{\partial \rho} \quad \text{for } r = 1 \quad (42)$$

The pressure is computed from

$$p(\theta) = p(0) + \frac{L}{R} \rho' \int_0^\theta \left(\frac{\partial \omega}{\partial \rho} \right) d\theta \quad \text{for } r = 1 \quad (13)$$

The pressure coefficient is defined by

$$C_p(\theta) = \frac{p(\theta) - p(0)}{\frac{1}{2} \rho (U_\infty^2 + V_\infty^2)} \quad (14)$$

The skin friction coefficient is computed from

$$C_f(\theta) = - \frac{2}{R} \omega \Big|_{r=1} \quad (15)$$

The force coefficients normal and tangential to the airfoil chords are denoted by C_N and C_T . The lift, drag, and moment coefficients are denoted respectively by C_L , C_D , and C_M , and are computed from C_p and C_f values.

Numerical Procedure

The grid system in the ρ - θ plane is formed by using $\Delta\rho = 1/47$ and $\Delta\theta = \pi/40$. These values are identical to those of Reference 7. As shown in Figure 2, the coordinates of the grid point i,j are $\rho = 1.0 - (j - 1) \Delta\rho$ and $\theta = (i - 1) \Delta\theta$. That is, the unit circle, $\rho = 1$, which corresponds to the airfoil surface in the physical plane, is assigned the value $j = 1$, the point $\rho = 0$, which corresponds roughly to a circle of radius $1/3 L$ in the physical plane, is assigned the value $j = 48$, the leading edge line is assigned the value $i = 41$, the trailing edge line is assigned the values $i = 1$ or 81 , as shown in Figure 1. Values of ω , $\partial\psi/\partial\rho$, and $\partial\psi/\partial\theta$ are computed at the grid

points i, j . Values of ψ , however, are computed midway between the grid points i, j and $i+1, j$, as shown in Figure 2 and designated $\psi_{i,j}$.

For the kinetic part of the computation, the vorticity transport equation, (19), is solved using finite difference methods. Both the ADI (alternating direction implicit) method and the SLR (successive line relaxation) method have been studied.

With the ADI method, central differences are used for the diffusion term. For the convection term, four different differencing schemes have been tried. These are: (1) central differences, (2) second upwind differences (Reference 10), (3) combination of the first two (Reference 11), and (4) selective central or upwind differences depending on the cell Reynolds number (Reference 12). Scheme (1) gives spurious values of vorticity near the outer edge of rotational region around $\theta = \Delta\theta$. Schemes (2) and (3) give unsatisfactory C_p distribution on the lower surface near the forward stagnation point. Scheme (4) is found to be better than the other three from these respects.

Using Scheme (4), the finite difference form of the vorticity transport equation is

$$\begin{aligned}
 r^2 H^2 \left[\frac{\omega_{i,j}^{n+\frac{1}{2}} - \omega_{i,j}^n}{\frac{1}{2}\Delta t} \right] &= \frac{L}{R} r_j (\rho' j + r_j \rho'' j) \frac{1}{2\Delta\rho} (\omega_{i,j-1}^n - \omega_{i,j+1}^n) \\
 &+ \frac{L}{R} (r_j \rho' j)^2 \cdot \frac{1}{(\Delta\rho)^2} (\omega_{i,j-1}^n - 2\omega_{i,j}^n + \omega_{i,j+1}^n) \\
 &+ \frac{L}{R} \frac{1}{(\Delta\theta)^2} (\omega_{i-1,j}^{n+\frac{1}{2}} - 2\omega_{i,j}^{n+\frac{1}{2}} + \omega_{i+1,j}^{n+\frac{1}{2}})
 \end{aligned}$$

$$+ (C_{\theta})_{i,j}^{n+\frac{1}{2}} + (C_{\rho})_{i,j}^n \quad (46)$$

and

$$\begin{aligned} r_j^2 H^2 \left[\frac{\omega_{i,j}^{n+1} - \omega_{i,j}^{n+\frac{1}{2}}}{\frac{1}{2}\Delta t} \right] &= \frac{L}{R} r_j (\rho'_j + r_j \rho''_j) \frac{1}{2\Delta\rho} (\omega_{i,j-1}^{n+1} - \omega_{i,j+1}^{n+1}) \\ &+ \frac{L}{R} (r_j \rho'_j)^2 \frac{1}{(\Delta\rho)^2} (\omega_{i,j-1}^{n+1} - 2\omega_{i,j}^{n+1} + \omega_{i,j+1}^{n+1}) \\ &+ \frac{L}{R} \frac{1}{(\Delta\theta)^2} (\omega_{i-1,j}^{n+\frac{1}{2}} - 2\omega_{i,j}^{n+\frac{1}{2}} + \omega_{i,j+1}^{n+\frac{1}{2}}) \\ &+ (C_{\theta})_{i,j}^{n+\frac{1}{2}} + (C_{\rho})_{i,j}^{n+1} \end{aligned} \quad (47)$$

Here, C_{θ} and C_{ρ} are the finite difference form of the convection terms. These terms are written out as explained below.

Two cell Reynolds's numbers based on the cell lengths in the θ and ρ direction are defined respectively as

$$(R_{C_{\theta}})_{i,j} = r_j \rho'_j \left| \frac{\partial \psi}{\partial \rho} \right|_{i,j} \frac{R}{L} \Delta\theta \quad (48)$$

and

$$(R_{C_{\rho}})_{i,j} = \frac{1}{r_j} \left| \frac{\partial \psi}{\partial \theta} \right|_{i,j} \frac{R}{L} (\Delta r)_j \quad (49)$$

If the value of $R_{C_\theta} < 2$, central difference is used for the term C_θ ; otherwise upwind difference is used. Similarly, central difference for the term C_ρ is used if $R_{C_\rho} < 2$; otherwise upwind difference is used. These differences are given below:

$$R_{C_\theta} < 2: \quad (C_\theta)_{ij} = (r\rho')_{ij} \frac{1}{2\Delta\theta} [(\psi_p w)_{i+1,j} - (\psi_p w)_{i-1,j}] \quad (50)$$

$$R_{C_\theta} \geq 2: \quad (C_\theta)_{ij} = \begin{cases} r_j \rho'_j \psi_{\rho_{ij}} (w_{ij} - w_{i-1,j}) \frac{1}{\Delta\theta}, & \text{if } \psi_{\rho_{ij}} < 0 \\ r_j \rho'_j \psi_{\rho_{ij}} (w_{i+1,j} - w_{ij}) \frac{1}{\Delta\theta}, & \text{if } \psi_{\rho_{ij}} > 0 \end{cases} \quad (51)$$

$$R_{C_\rho} < 2: \quad (C_\rho)_{ij} = -r_j \rho'_j \frac{1}{2\Delta\rho} [(\psi_\theta w)_{i,j-1} - (\psi_\theta w)_{i,j+1}] \quad (52)$$

$$R_{C_\rho} \geq 2: \quad (C_\rho)_{ij} = \begin{cases} -r_j \rho'_j (\psi_\theta)_{ij} (w_{ij} - w_{i,j+1}) \frac{1}{\Delta\rho}, & \text{if } \psi_\theta > 0 \\ -r_j \rho'_j \psi_{\theta_{ij}} (w_{i,j-1} - w_{ij}) \frac{1}{\Delta\rho}, & \text{if } \psi_\theta < 0 \end{cases} \quad (53)$$

In the above set of relations, the superscripts for w indicating the time step are as determined by equation (46) and (47). As of now, the stream function and its derivatives are allowed to lag by one time step and so the superscripts for ψ_ρ and ψ_θ are always n , irrespective of what is implied by equations (46) and (47).

The solution procedure is as follows. For each value of j , equation (46) gives a set of 80 algebraic equations involving 80 unknown values of vorticity at the 80 grid points "i" on the grid lines and at the time level $(n + \frac{1}{2})$. The coefficient matrices for these sets of

algebraic equations is cyclic tridiagonal. Recursion relations (Reference 13) are utilized to solve the sets of algebraic equation for each pertinent j value, beginning with $j = 2$ and ending with the first " j " grid line where the vorticity is zero at each grid point " i " at the time level n .

Equation (47) is then solved to obtain the vorticity values at the time level $n + 1$. For each value of i , equation (47) gives a set of algebraic equations involving unknown vorticity values at the grid points " j " and at the time level $(n + 1)$. There are 80 sets of algebraic equations, one set for each for each value of i . The coefficient matrices are regular tridiagonal and Thomas algorithm (Reference 10) is used. It should be noted that the solution requires the surface vorticity at the $(n + 1)$ th time level be known. The surface vorticity values at the $(n + 1)$ th time level, however, depends on the vorticity values away from the surface kinematically, as discussed earlier. An iterative procedure is therefore adopted with which the surface vorticity values computed from the kinematic relation, equation (39), based on non-surface vorticity values obtained for each iteration are used in the subsequent iteration. For the initial iteration, the surface vorticity values are estimated from the surface vorticity values at time levels $(n-1)$ and n through an extrapolation procedure.

For the successive line relaxation scheme, using central differences for the space derivatives and forward differences for the time derivative, the residue is written as

$$(\Delta\omega)_{ij}^{n+1,k+1} = \omega_{ij}^{n+1,k+1} - \omega_{ij}^{n+1,k}$$

$$\begin{aligned}
&= \omega_{ij}^n + \frac{\Delta t}{rH^2} \left[C_1 (\omega_{i,j+1}^{n+1,k+1} - 2\omega_{ij}^{n+1,k+1} + \omega_{i,j-1}^{n+1,k+1}) \right. \\
&+ C_2 (\omega_{i,j-1}^{n+1,k+1} - \omega_{i,j+1}^{n+1,k+1}) + C_3 (\omega_{i+1,j}^{n+1} - 2\omega_{ij}^{n+1} - \omega_{i-1,j}^{n+1}) \\
&\quad \left. + C_4 (\psi_{\rho_{i+1,j}}^n \omega_{i+1,j}^{n+1} - \psi_{\rho_{i-1,j}}^n \omega_{i-1,j}^{n+1}) \right. \\
&\quad \left. + C_5 (\psi_{\theta_{i,j-1}}^n \omega_{i,j-1}^{n+1,k+1} - \psi_{\theta_{i,j+1}}^n \omega_{i,j+1}^{n+1,k+1}) \right] - \omega_{ij}^{n+1,k} \quad (54)
\end{aligned}$$

where k is the iteration counter.

$$\begin{aligned}
C_1 &= \frac{L}{R} \frac{[r\rho'^2]_j}{(\Delta\rho)^2} ; C_2 = \frac{L}{R} \frac{(\rho + r\rho'')_j}{2\Delta\rho} ; C_3 = \frac{1}{rj} \frac{L}{R} \frac{1}{(\Delta\theta)^2} \\
C_4 &= \frac{\rho'_j}{2\Delta\theta} ; C_5 = \frac{\rho'_j}{2\Delta\rho}
\end{aligned}$$

The iteration counters for the vorticity values on grid lines $i + 1$ and $i - 1$ in equation (48) are specified in accordance with the direction of sweep. The sweeps always initiate with the grid line $i = 41$ (the leading edge line) and terminate with the grid line $i = 81$ (or 1). Thus, for the upper surface of the airfoil, the sweep is in the $i \uparrow$ direction, i.e., $i:41(1) 81$. The iteration counter for vorticity values is $k + 1$ on the grid line $i - 1$ and is k on the grid line $i + 1$. For the lower surface, the sweep is in the $i \downarrow$ direction, i.e., $i:41(-1)1$. The iteration counter for vorticity values is $k + 1$ on the grid line

$i + 1$ and is k on the grid line i . The order in which the upper and lower surface sweeps are done is alternated for successive iterations. For odd numbered iterations, the sweep along the upper surface is followed by the sweep along the lower surface. For even numbered iterations, the sweep along the lower surface is undertaken before the sweep along the upper surface.

With the above procedure, a system of algebraic equations with a tridiagonal coefficient matrix is obtained from equation (54) for each value of i . These equations are solved for values of $\omega_{i,j}^{n+1,k+1}$ not on the airfoil surface. The corresponding values of surface vorticity are obtained by solving equation (39). The values of ω at all grid points are then re-set using the equation

$$\omega_{i,j}^{n+1,k+1} = \omega_{i,j}^{n+1,k} + \beta(\Delta\omega)_{i,j}^{n+1,k+1} \quad (55)$$

where β is the relaxation parameter and is assigned the value of 0.09.

The calculations with successive line relaxation, were repeated using Arakawa difference for the convection terms and three-point backward difference for the time derivative. The results presented here are obtained using Arakawa and three-point backward differences.

The method of computation of loads is identical to that of Reference 7.

Discussion of Results

Solutions using ADI method have been obtained up to a time level of $t = 0.212$ and using SLR method up to $t = 0.02$. Figures 3 to 8 show the vorticity profiles at several chordwise stations obtained using

the ADI method and the SLR method. A comparison of these solutions with those of Reference 7 shows that the ADI solution agrees well with the SLR solution and the solution given in Reference 7 at stations away from the trailing edge (Figures 3, 4, 5 and 8). At the trailing edge station (Figure 6 and 7) the ADI solution differs substantially from that of Reference 7. In particular, the slope of the vorticity profile changes drastically and repeatedly near the surface (Figure 6) so that no meaningful computation of the normal vorticity gradient at the trailing edge is possible. This erratic behavior, in fact, extends to chordwise stations near the trailing edge. In addition to the erratic instantaneous behavior near the trailing edge described above, it is found (although not shown here) that the vorticity values near the trailing edge as obtained by the ADI method oscillate violently as time progresses. As a consequence, no reliable surface pressure distribution, which must be computed from the normal velocity gradients, can be established from the ADI solution near the trailing edge.

The vorticity profiles at the trailing edge as obtained from the SLR method are in good qualitative agreement with that of Reference 7. Quantitatively, there are noticeable differences between the two solutions near the surface which increases gradually with the progression of time. These differences are not unexpected since the method of determining the surface vorticity in the present study is substantially different from that of Reference 7.

The surface pressure distribution for $\delta = 0.003$, 0.006 and 0.02 are plotted in Figures 9, 11 and 13. For the ADI solution the mean of

clockwise and anti-clockwise integration is plotted. In the case of SLR solution the results presented correspond to integration from the leading edge along the upper and lower surfaces. In addition, the values are plotted so as to make the leading edge C_p same in all cases. The values of the constant added to achieve this, are indicated in the figures. Figures 10 and 12 give the C_p distribution close to the trailing edge. Values of results obtained by Mehta are not included in these figures, as they are not available in such detail in Reference 7. As could be seen from Figures 9-13, the ADI method gives rise to meaningless values of C_p near the trailing edge. The ADI solution gives C_p curves that are not closed. That is, after the completion of a circuit around the airfoil the starting value of C_p is not returned. This is due to the erroneous values of the vorticity gradient at the surface as predicted by ADI method. The ADI solution deteriorates further with time and gives rise to negative lift as could be seen from Figure 13.

The SLR results for C_p are obtained by integrating from the leading edge along the upper and lower surface. This gives rise to two values of C_p for the trailing edge. We define a ΔC_p obtained by dividing the difference between these two values by the maximum absolute value of C_p on the surface. A comparison of these values with those of Reference 7 is as indicated below.

<u>Time Block</u>	<u>No. of Time Steps</u>	<u>%ΔC_p, Average</u>	
		<u>Present Study, SLOR</u>	<u>Mehta</u>
0.0 → 0.006	6	2.161	1.468
0.006 → 0.012	3	0.640	1.593
0.012 → 0.02	2	0.400	1.082

The variation of C_j with time, for SLR scheme, is given in Figure 14. Compared to results of Reference 7, these values show a smoother variation with time.

From the above discussion it is concluded that successive over-relaxation is to be preferred over ADI method. As of now, the exact cause of the failure of the ADI method is not known. Unfortunately, the SOR method is more time consuming than ADI scheme. It may be possible to reduce the computer time for the SOR method by choosing a set of optimum relaxation parameters which has a spacewise variation. These conclusions are based on a few numerical experiments carried out in advancing the solution from $t = 0.002$ to $t = 0.003$. The following table summarizes the findings.

<u>Scheme</u>	<u>No. of Iterations</u>	<u>Computation Time (sec)</u>
1. ADI	40	81
2. Point SOR	125	178
3. Line SOR with $\beta = 0.09$	74	149
4. Line SOR with $\beta_j = 1.5 \sqrt{(\Delta x)_j}$	60	127

In the above experiments, the convergence tolerance on Δu has been kept same at 0.5. In the ADI scheme the iteration indicated is for the surface vorticity during r-direction sweep. It is apparent that successive line over-relaxation has a slight advantage over successive point over-relaxation. The relation for β_j given in item 4 above is an ad hoc selection and has no theoretical basis.

In continuing this work, a proper investigation of the relaxation

factor for SLR method is to be done. There is also a possibility of combined usage of ADI and SLR schemes, with the successive over-relaxation scheme limited to a small region near the trailing edge. This possibility is still to be explored.

REFERENCES

1. J. C. Wu, A. H. Spring, and N. J. Sankar, "A Flowfield Segmentation Method for the Numerical Solution of Viscous Flow Problems," Proceedings of the Fourth International Conference on Numerical Methods in Fluid Dynamics, pp. 452-457, Springer-Verlag, 1975.
2. J. C. Wu, "Integral Representation of Field Variables for the Finite Element Solution of Viscous Flow Problems," Proceedings of the 1974 Conference on Finite Element Methods in Engineering, pp. 827-840, Clarendon Press, 1974.
3. J. C. Wu, "Velocity and Extraneous Boundary Conditions of Viscous Flow Problems," AIAA paper 75-47, 1975.
4. J. C. Wu, "Division of Computation Field for the Finite Element Method," Finite Element Methods in Flow Problems, J. T. Oden et. al., Editors, pp. 769-776, UAH Press, 1975.
5. J. C. Wu and J. F. Thompson, "Numerical Solutions of Time-Dependent Incompressible Navier-Stokes Equations using an Integro-Differential Formulation," Computers and Fluids, Vol. 1, pp. 197-215, 1973.
6. J. F. Thompson, S. P. Shanks, and J. C. Wu, "Numerical Solution of Three-Dimensional Navier-Stokes Equations Showing Trailing Tip Vortices," AIAA Journal, Vol. 12, pp. 787-794, 1974.
7. U. B. Mehta, "Starting Vortex, Separation Bubbles and Stall - A Numerical Study of Laminar Unsteady Flow Around an Airfoil," Ph.D. Thesis, Illinois Institute of Technology, Chicago, 1972.
8. M. J. Lighthill, "Vorticity and the Development of Fluid Flows," Laminar Boundary Layers, L. Rosenhead, Editor, pp. 46-59, Oxford University Press, 1963.
9. A. Sommerfeld, Partial Differential Equations in Physics, Academic Press, 1949.
10. P. J. Roache, Computational Fluid Dynamics, Hermosa Publishers, 1972.
11. R. T. Davis, "Numerical Solution of Laminar Incompressible Flow Past a Parabola," J. Fluid Mech., Vol. 51, pp. 417-433.
12. A. K. Rundal, "Convergence and Accuracy of Three Finite Difference Schemes for a Two-dimensional Conduction and Convection Problem" International Journal for Numerical Methods in Engineering, Vol. 4, pp. 541-550.

13. D. J. Evans and L. V. Atkinson, "An Algorithm for the Solution of General Three Term Linear Systems," *Computer Journal*, No. 13, pp. 323-324.

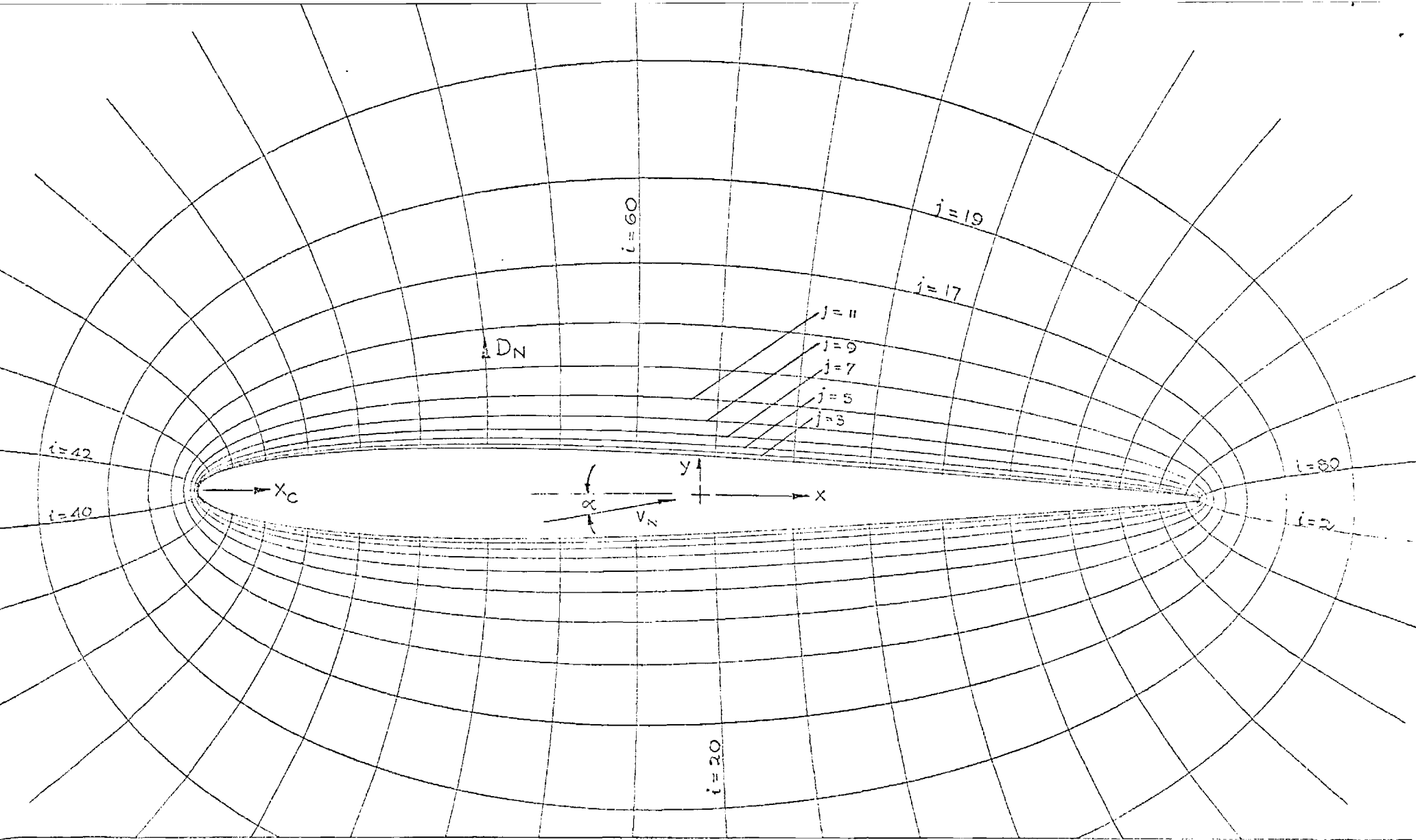
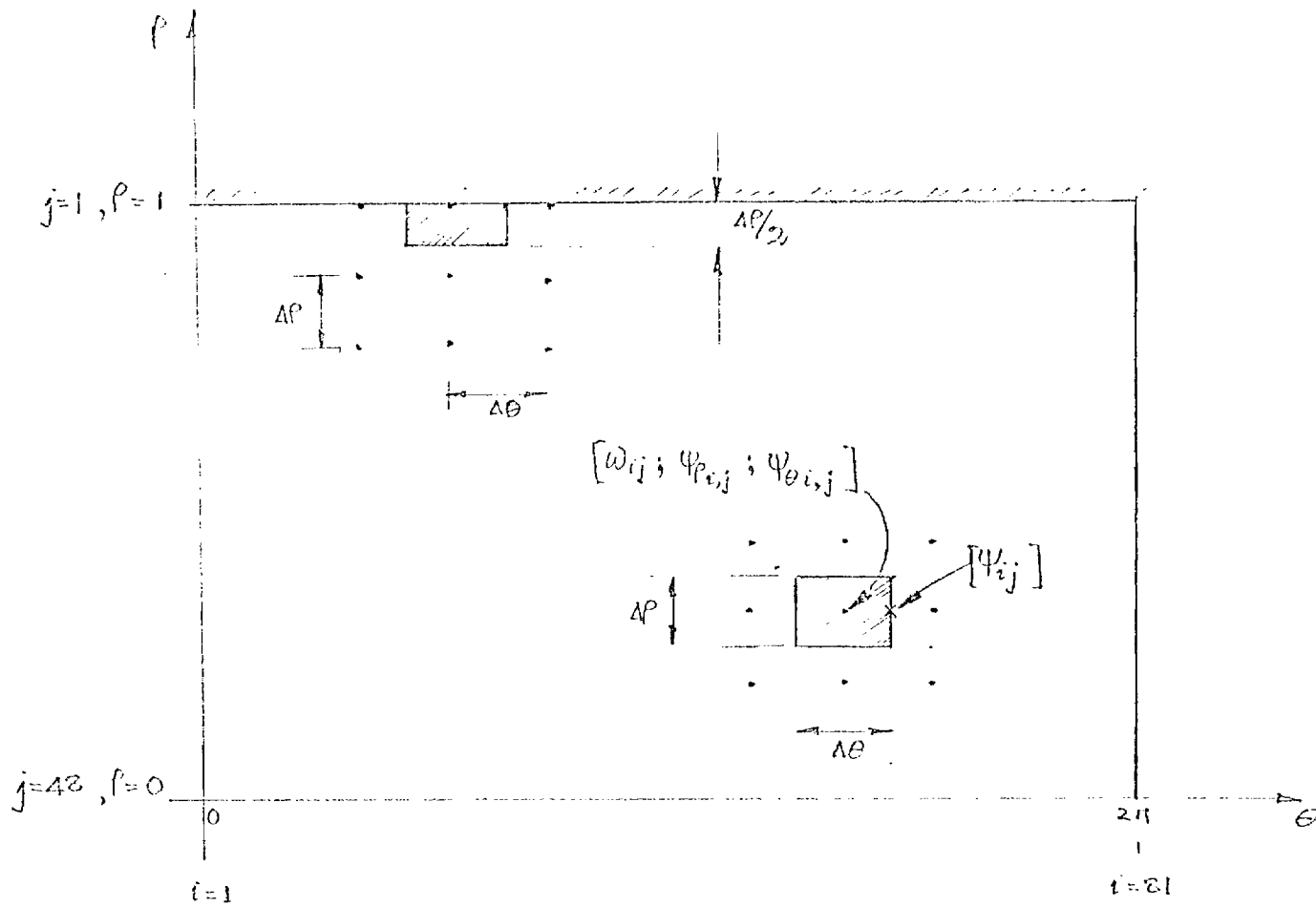


FIG 1. THE GRID SYSTEM IN PHYSICAL PLANE



NOTE: THE INDEX j INCREASES WITH DECREASING r .

$$r_j = 1.0 - (j-1) \Delta r$$

$$\theta_i = (i-1) \Delta \theta$$

FIG. 2. THE GRID SYSTEM IN THE WORKING PLANE.

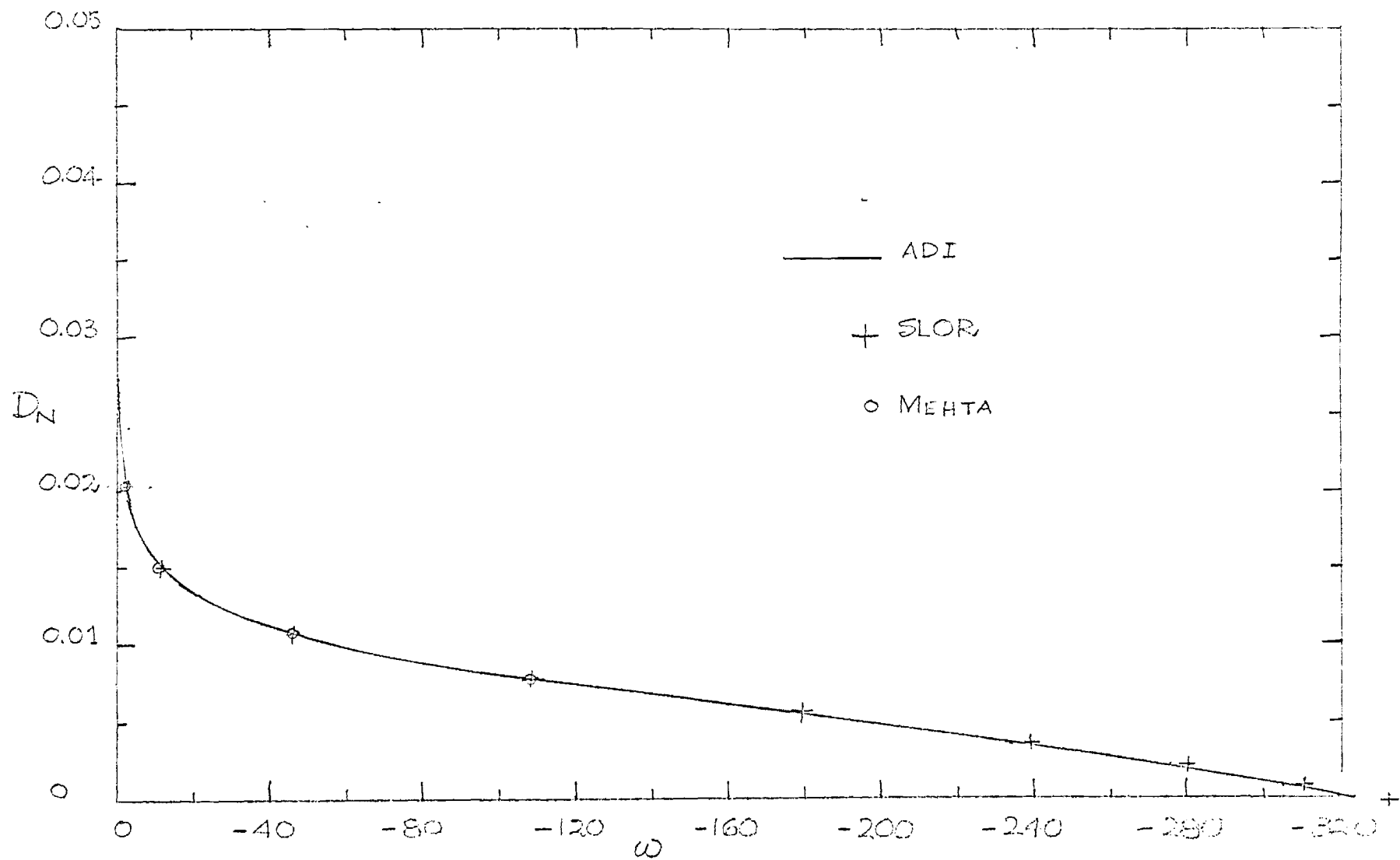


FIG. 3 VORTICITY PROFILE AT $X_C = 0.0$; $t = 0.006$

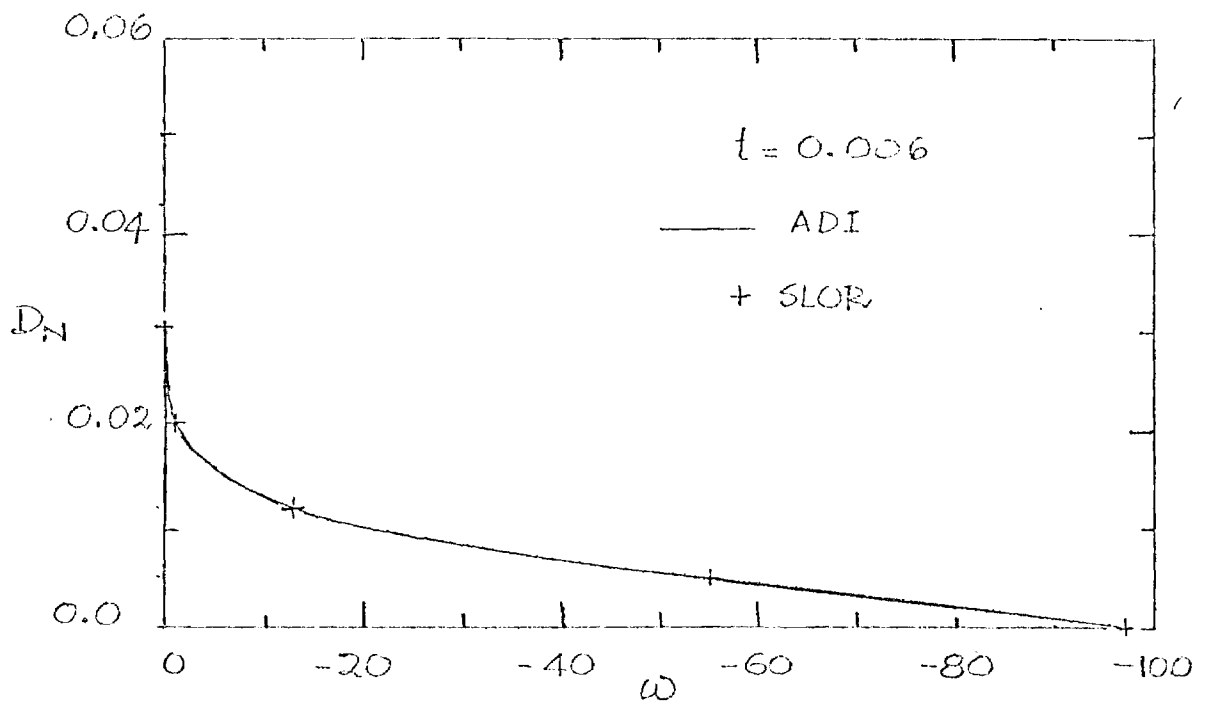


FIG. 4. VORTICITY PROFILE AT $X_{CU} = 0.8406$

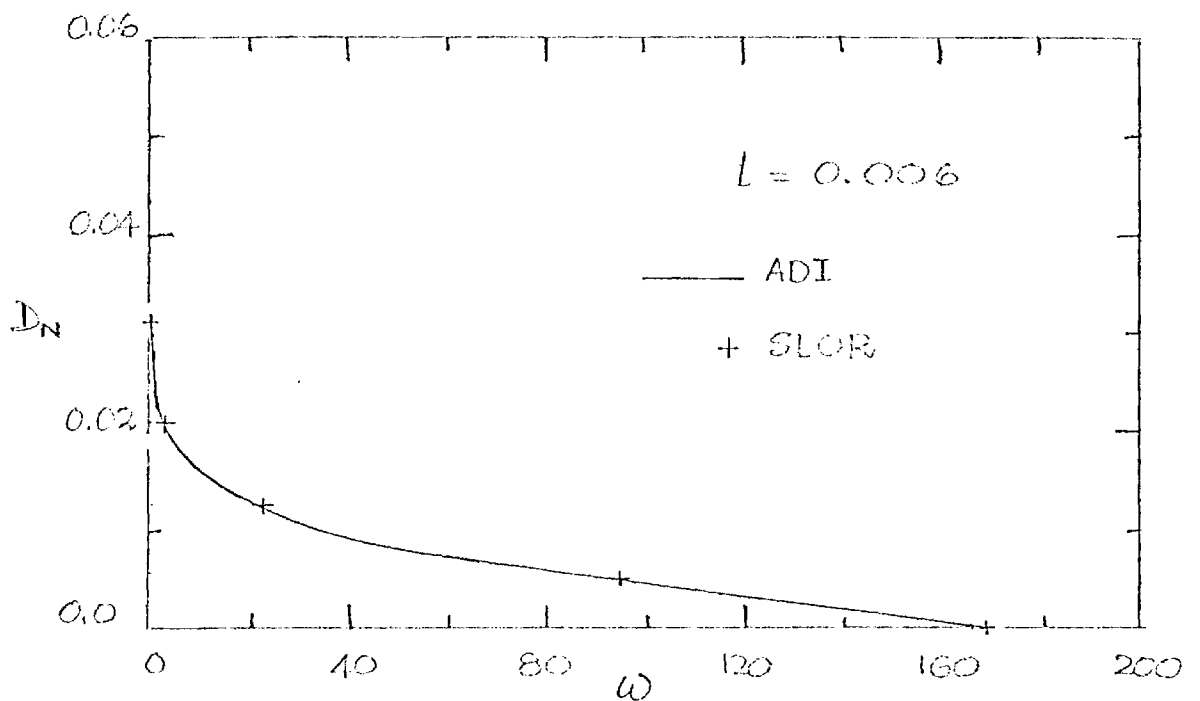


FIG. 5. VORTICITY PROFILE AT $X_{CL} = 0.8406$

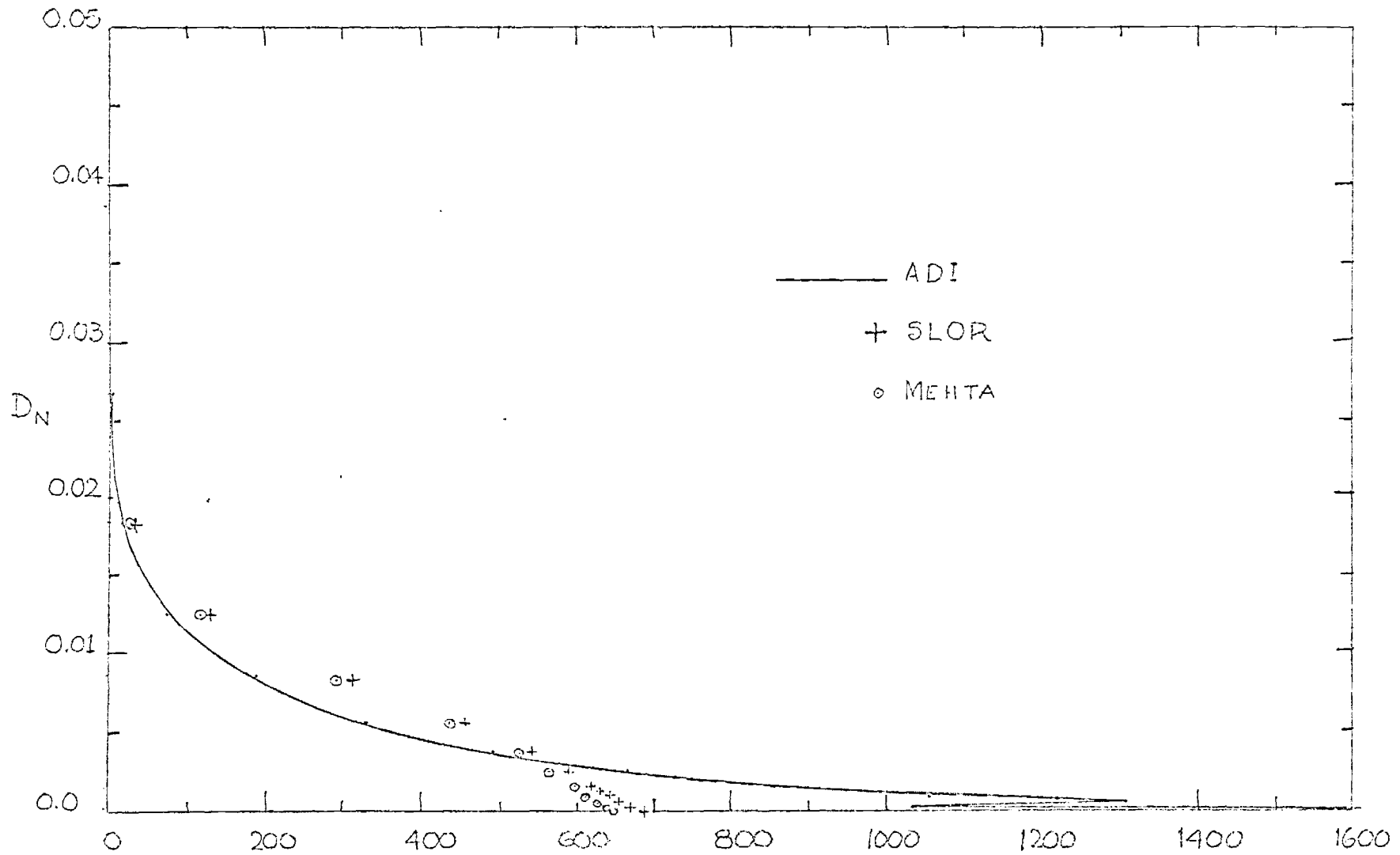


FIG. 6. VORTICITY PROFILE AT $X_c = 1.0$; $t = 0.006$

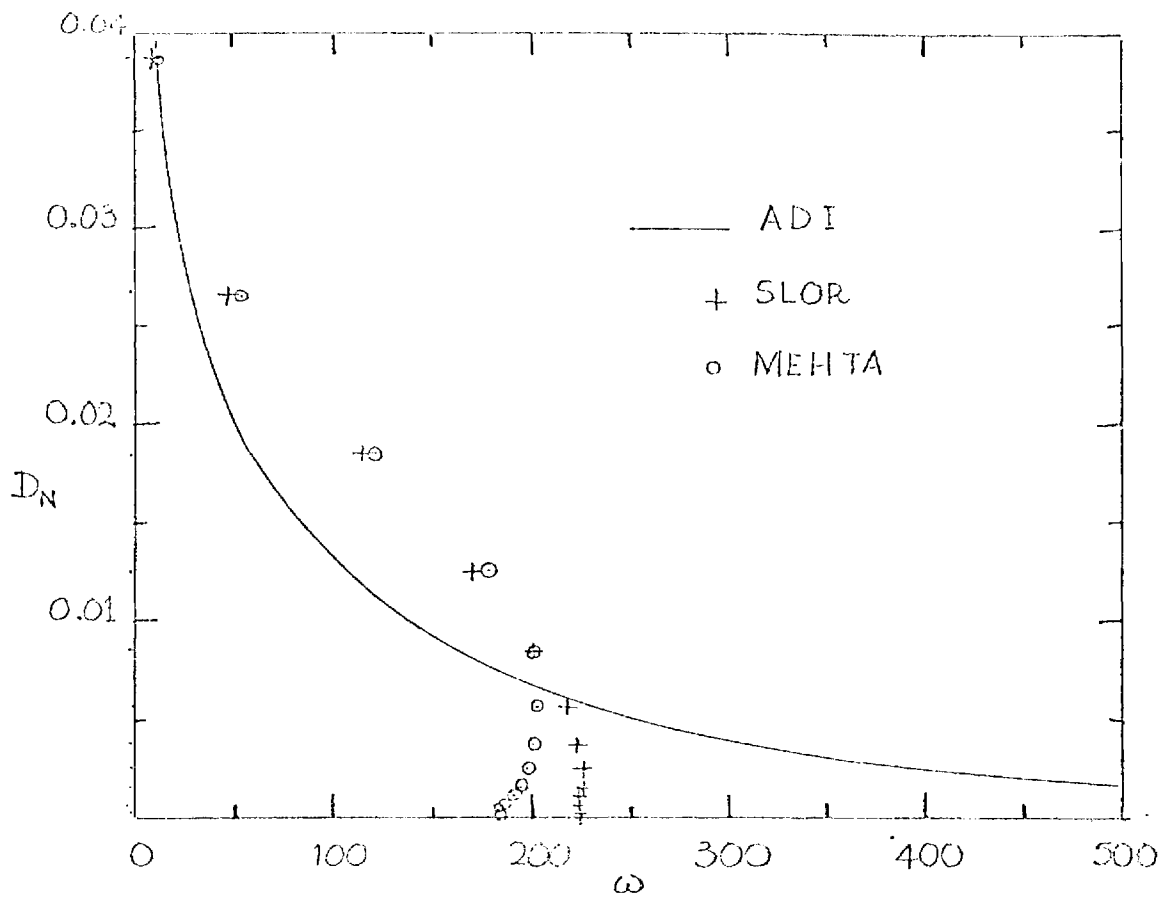


FIG.7 VORTICITY PROFILE AT $X_C = 1.0$; $t = 0.02$

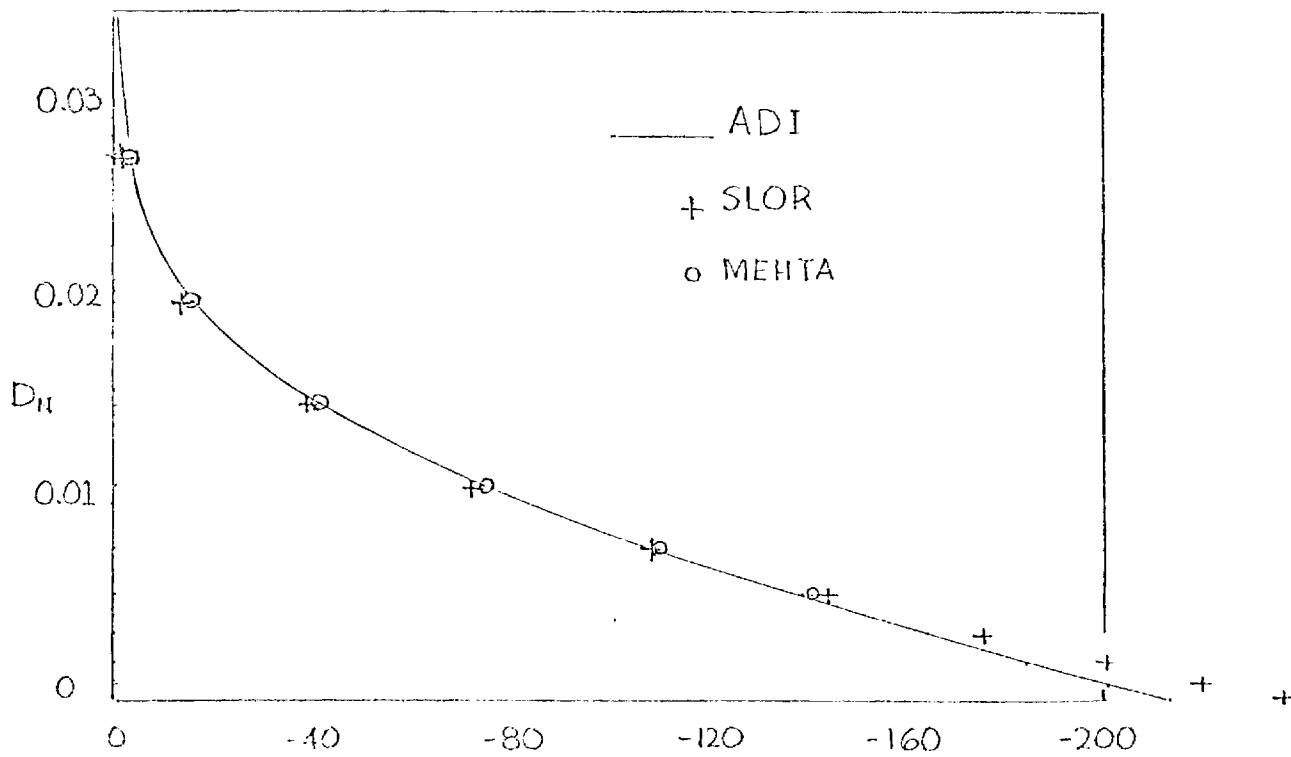


FIG.8 VORTICITY PROFILE AT $X_C = 0.0$; $t = 0.02$

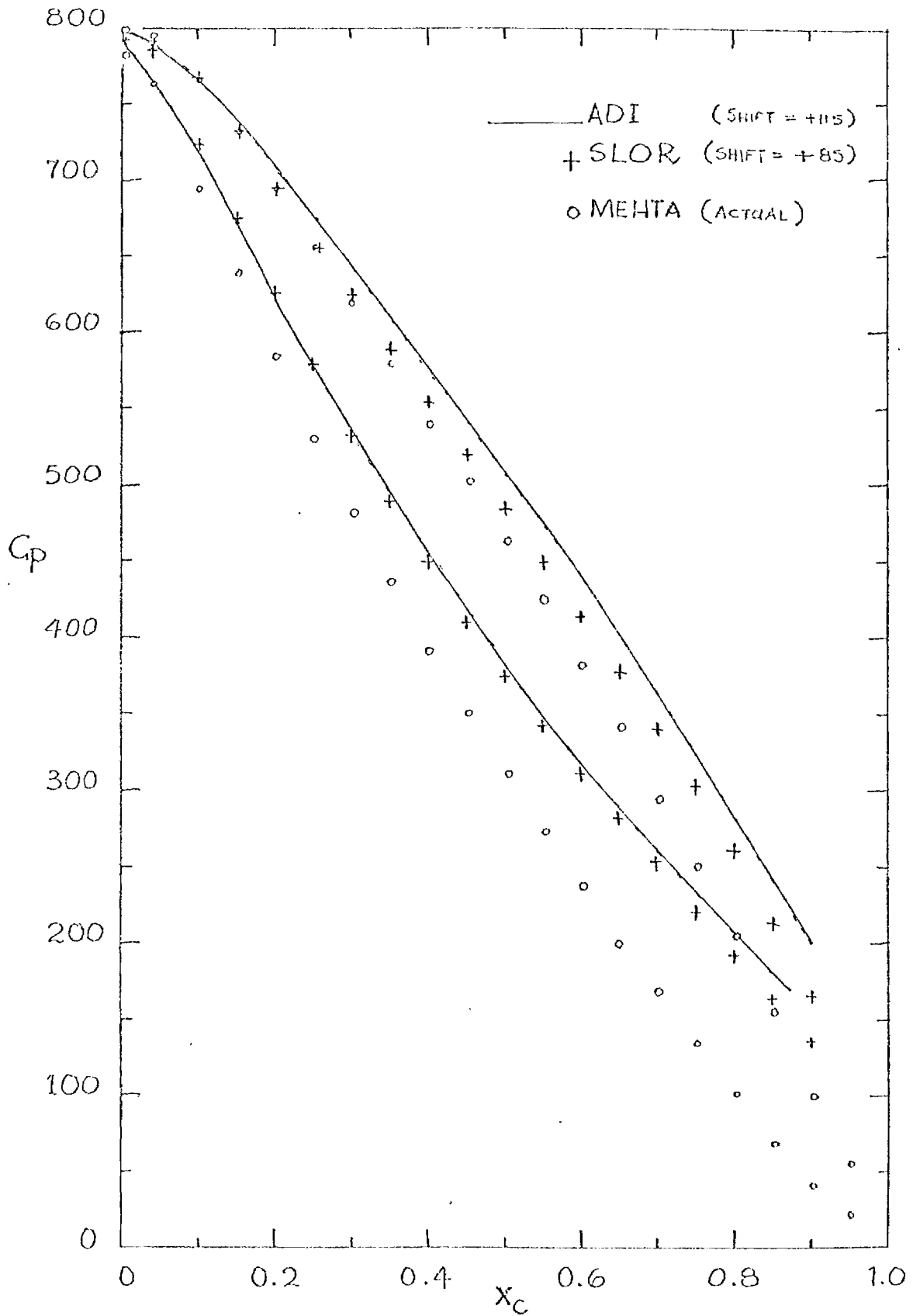


FIG. 9. SURFACE PRESSURE DISTRIBUTION
 $t = 0.003$

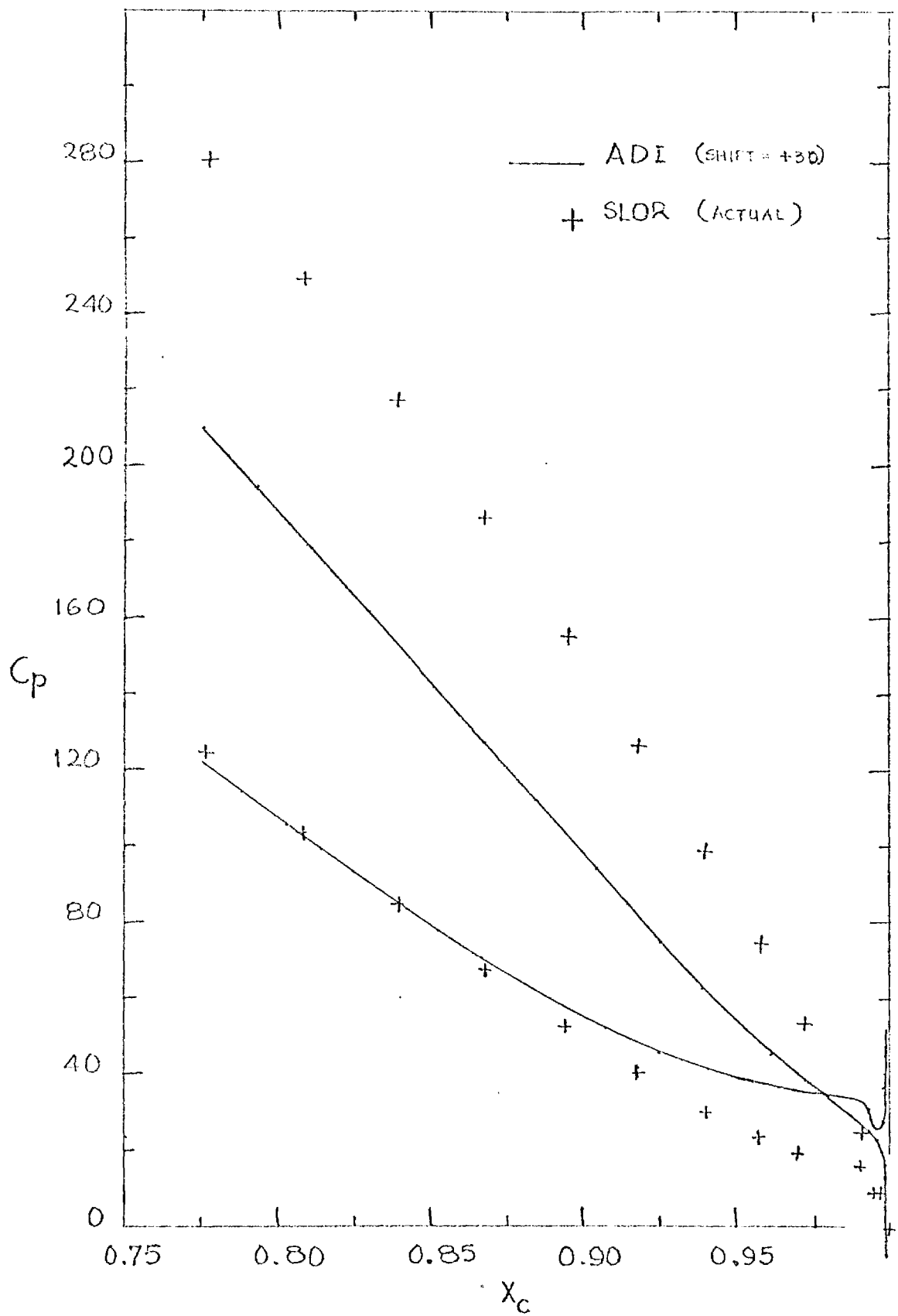


FIG. 10 SURFACE PRESSURE DISTRIBUTION
NEAR TRAILING EDGE

$$t = 0.003$$

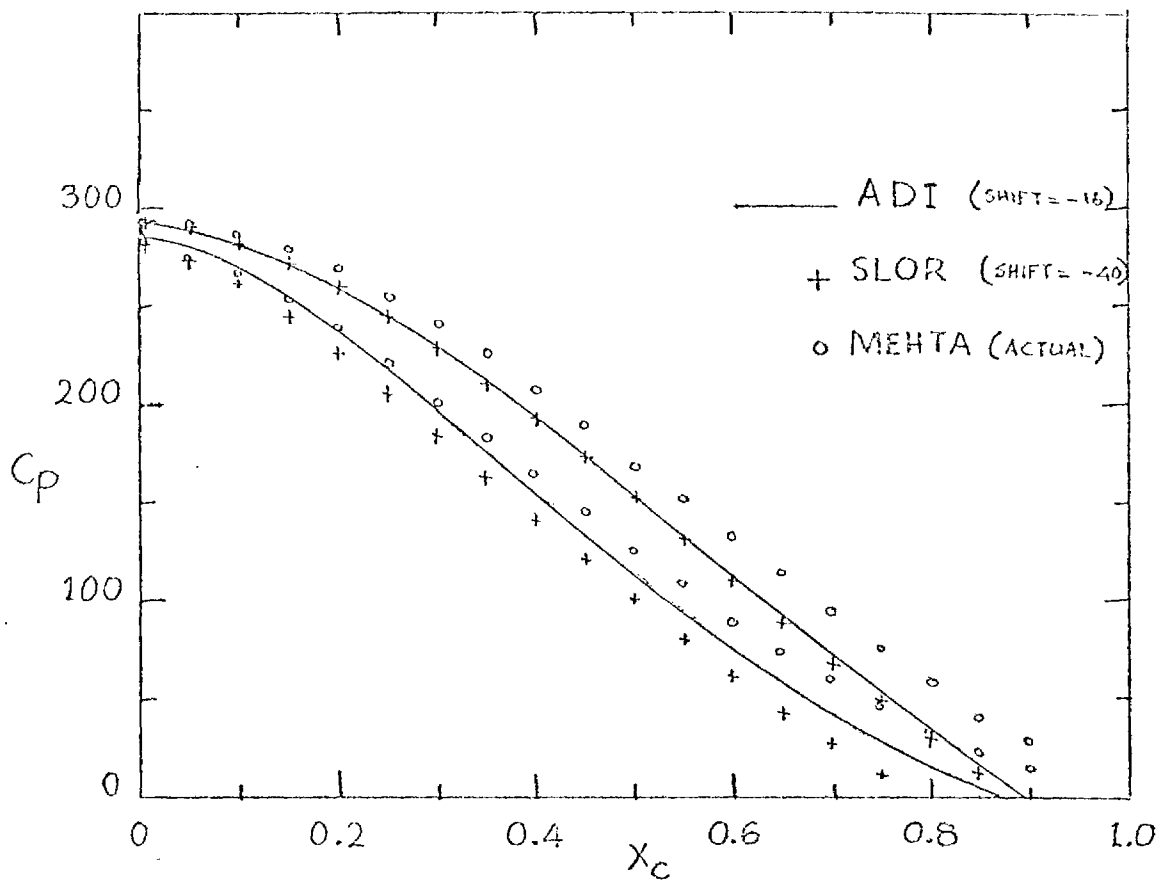


FIG.11 SURFACE PRESSURE DISTRIBUTION AT $t = 0.006$

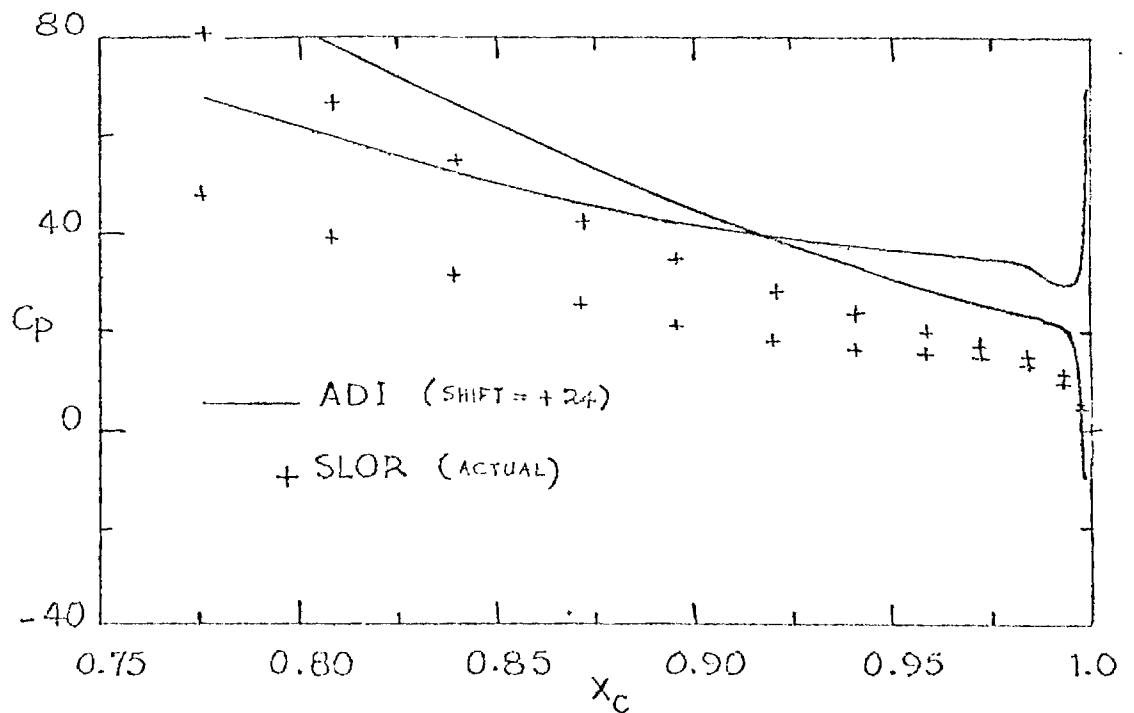


FIG.12 SURFACE PRESSURE DISTRIBUTION
NEAR TRAILING EDGE $t = 0.006$

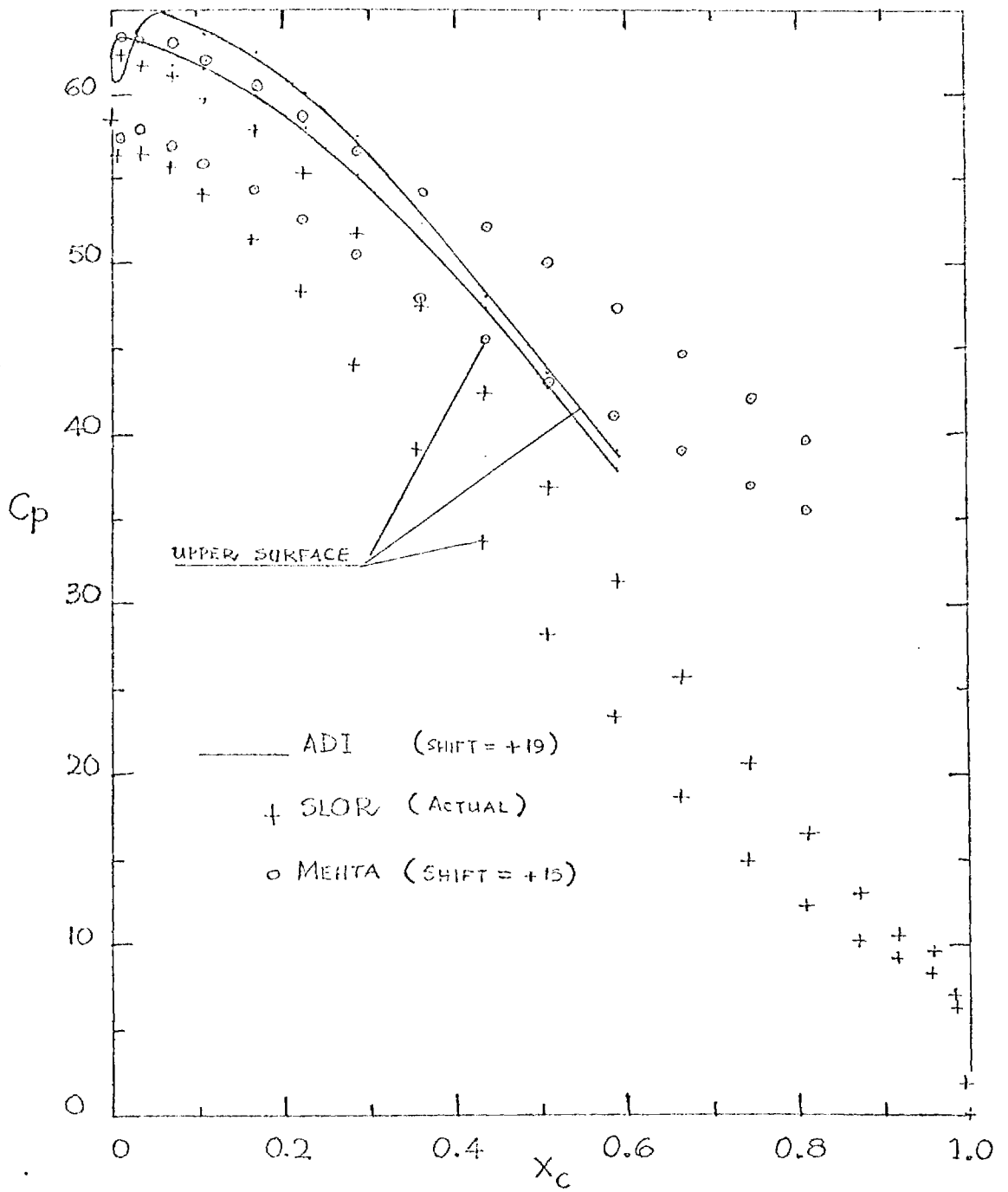


Fig.13 SURFACE PRESSURE DISTRIBUTION AT $t=0.02$

FIG. 14 VARIATION OF LIFT COEFF. WITH TIME.

